

1 **LIVAS: a 3D multi-wavelength aerosol/cloud database based**
2 **on CALIPSO and EARLINET**

3 **V. Amiridis¹, E. Marinou¹, A. Tsekeri¹, U. Wandinger², A. Schwarz², E. Gianna-**
4 **kaki³, R. Mamouri⁴, P. Kokkalis¹, I. Biniotoglou⁵, S. Solomos¹, T. Herekakis¹, S.**
5 **Kazadzis⁶, E. Gerasopoulos⁶, E. Proestakis¹, D. Balis⁷, A. Papayannis⁸, C.**
6 **Kontoes¹, K. Kourtidis⁹, N. Papagiannopoulos¹⁰, L. Mona¹⁰, G. Pappalardo¹⁰, O.**
7 **Le Rille¹¹ and A. Ansmann²**

8 [1] {Institute for Astronomy, Astrophysics, Space Applications and Remote Sensing,
9 National Observatory of Athens, Athens, 15236, Greece; tel: +302108109196, fax:
10 +302106138343}

11 [2] {Leibniz Institute for Tropospheric Research (TROPOS), Leipzig, Germany}

12 [3] {Finnish Meteorological Institute, Kuopio Unit, Finland}

13 [4] {Cyprus University of Technology, Limassol, Cyprus}

14 [5] {National Institute of R&D for Optoelectronics, Bucharest, Romania}

15 [6] {Institute of Environmental Research and Sustainable Development, National Ob-
16 servatory of Athens, Greece}

17 [7] {Aristotle University of Thessaloniki, Thessaloniki, Greece}

18 [8] {National Technical University of Athens, Zografou, Greece}

19 [9] {School of Engineering, Democritus University of Thrace}

20 [10] {Istituto di Metodologie per l'Analisi Ambientale, Consiglio Nazionale delle Ri-
21 cerche, Potenza, Italy}

22 [11] {European Space Agency}

23 Correspondence to: Vassilis Amiridis (vamoir@noa.gr)

1 **Abstract**

2 We present LIVAS, a 3-dimensional multi-wavelength global aerosol and cloud opti-
3 cal database, optimized to be used for future space-based lidar end-to-end simulations
4 of realistic atmospheric scenarios as well as retrieval algorithm testing activities.
5 LIVAS database provides averaged profiles of aerosol optical properties for the poten-
6 tial space-borne laser operating wavelengths of 355, 532, 1064, 1570 and 2050 nm
7 and of cloud optical properties at the wavelength of 532 nm. The global database is
8 based on CALIPSO observations at 532 and 1064 nm and on aerosol-type-dependent
9 backscatter- and extinction-related Ångström exponents, derived from EARLINET
10 ground-based measurements for the UV and scattering calculations for the IR wave-
11 lengths, using a combination of input data from AERONET, suitable aerosol models
12 and recent literature. The required spectral conversions are calculated for each of the
13 CALIPSO aerosol types and are applied to CALIPSO backscatter and extinction data
14 correspondingly to the aerosol type retrieved by the CALIPSO aerosol classification
15 scheme. A cloud optical database based on CALIPSO measurements at 532 nm is also
16 provided, neglecting wavelength conversion due to approximately neutral scattering
17 behavior of clouds along the spectral range of LIVAS. Averages of particle linear de-
18 polarization ratio profiles at 532 nm are provided as well. Finally, vertical distribu-
19 tions for a set of selected scenes of specific atmospheric phenomena (e.g. dust out-
20 breaks, volcanic eruptions, wild fires, polar stratospheric clouds) are analyzed and
21 spectrally converted so as to be used as case studies for space-borne lidar performance
22 assessments. The final global dataset includes 4-year (01/01/2008 – 31/12/2011) time-
23 averaged CALIPSO data on a uniform grid of 1x1 degree with the original high verti-
24 cal resolution of CALIPSO in order to ensure realistic simulations of the atmospheric
25 variability in lidar end-to-end simulations.

26

1 **1. Introduction**

2 A general methodology to test the ability of candidate future space-borne remote-
3 sensing instruments to observe atmospheric quantities is the application of their pro-
4 cessing algorithms on simulated datasets. The datasets are usually based on the in-
5 strument characteristics and a description of the atmospheric state. Especially for ac-
6 tive remote sensors as lidars, the vertical dimension should be included in the simula-
7 tions. Global distributions of such data are available today due to the launch of the
8 Cloud-Aerosol Lidar with Orthogonal Polarization (CALIOP) instrument on board the
9 Cloud-Aerosol Lidar and Infrared Pathfinder Satellite Observations (CALIPSO) mis-
10 sion of NASA/CNES in June 2006 (Winker et al., 2009). Ever since, CALIPSO pro-
11 vides global aerosol and cloud vertical distributions to the scientific community
12 through analysis of CALIOP backscatter observations at the operating wavelengths of
13 532 and 1064 nm.

14 The technique of active remote sensing of the atmosphere by lidar has been also cho-
15 sen for two of the future ESA Earth Explorer Missions, namely the Atmospheric Dy-
16 namics Mission Aeolus (ADM-Aeolus, Stoffelen et al., 2005) and the Earth Clouds,
17 Aerosols and Radiation Explorer (EarthCARE, ESA-SP-1279(1); Illingworth et al.,
18 2014), and was further proposed for the Advanced Space Carbon and Climate Obser-
19 vation of Planet Earth (A-SCOPE), one of the candidates for the 7th Earth Explorer
20 mission. Atmospheric Laser Doppler Instrument (ALADIN) on-board ADM-Aeolus
21 and ATmospheric LIDar (ATLID) on-board EarthCARE are two High Spectral Reso-
22 lution Lidars (HSRLs) operating at 355 nm and detecting the backscatter signal from
23 atmospheric aerosols, clouds and molecules in order to retrieve the horizontal compo-
24 nent of the wind vector with Doppler techniques (ALADIN) and the vertical profiles
25 of aerosol and cloud backscatter, extinction and particle depolarization (ATLID). The

1 instrument design proposed for the A-SCOPE mission is an Integrated Path Differen-
2 tial Absorption (IPDA) lidar, aiming at measuring column-averaged dry-air CO₂ mix-
3 ing ratios with high precision and low bias error, based on Short-Wave Infrared
4 (SWIR) (1570 nm or 2050 nm) laser and detector technologies.

5 The ESA Reference Atmosphere Model (RMA) currently used for the design and the
6 performance validation of ALADIN and ATLID instruments is derived from airborne
7 lidar measurements performed at 10.6 μm over regions of the Atlantic during a rela-
8 tively clean atmospheric period (1988-1990, Vaughan et al., 1998). This RMA con-
9 sists of five statistical aerosol backscatter profiles organized by percentiles and one
10 molecular profile with a resolution of 0.5 km from 0 to 16 km altitude. ESA RMA
11 provides also the optical properties of various clouds and the albedos for different sur-
12 face types (sea/land/ice).

13 Due to its spatial restrictions, the current ESA RMA is not representative for global
14 simulations. The correct performance assessment of current and future ESA lidar in-
15 struments requires the development of a refined aerosol and cloud optical database
16 with high spatial resolution for the Planetary Boundary Layer (PBL), the free tropo-
17 sphere (FT) and the stratosphere. An appropriate RMA should be representative of
18 both statistical atmospheric information (i.e. per atmospheric region, climate zone and
19 season) and deterministic information (i.e. extended atmospheric scenes with, e.g.,
20 Saharan dust events, biomass-burning aerosol events, volcanic eruption events, polar
21 stratospheric cloud events, convective cloud events). Moreover, the RMA should in-
22 clude multi-wavelength parameters so as to cover the spectral domain of future HSRL
23 and IPDA lidar missions, specifically the three harmonic operating wavelengths of
24 Nd:YAG lasers (355, 532 and 1064 nm) and typical wavelengths of future IPDA li-
25 dars in the SWIR spectral domain (1.57 and 2.05 μm).

1 Over the recent years, the European Aerosol Research Lidar Network (EARLINET,
2 <http://www.earlinet.org/>, Pappalardo et al., 2014) and the Aerosol Robotic Network
3 (AERONET, <http://aeronet.gsfc.nasa.gov/>, Holben et al., 1998) ground-based lidar
4 and sunphotometer networks, respectively, along with the CALIPSO backscatter lidar
5 mission have provided new resources that can be used for the elaboration of such a
6 multi-wavelength database for typical laser operating wavelengths. Additionally, sev-
7 eral airborne and ground-based field experiments involving in-situ instrumentation
8 together with HSRL and multi-wavelength Raman lidar systems have been performed
9 over the last twenty years and can be very useful for the consolidation of such a RMA.
10 In this paper we present the “Lidar climatology of Vertical Aerosol Structure for
11 space-based lidar simulation studies” (LIVAS) which is a RMA aiming to provide
12 profiles of aerosol and cloud optical properties on a global scale, that can be used for
13 the simulation of realistic atmospheric scenarios in current and future lidar end-to-end
14 simulations and retrieval algorithm testing activities. For HSRL and IPDA lidar appli-
15 cations, LIVAS addresses the wavelength dependency of aerosol optical properties for
16 the following laser operating wavelengths: 355 nm, 532 nm, 1064 nm, 1.57 μm and
17 2.05 μm . Moreover, LIVAS includes regional and seasonal statistics of aerosol and
18 cloud extensive and intensive optical properties in terms of backscatter coefficient,
19 extinction coefficient and particle linear depolarization ratio. Furthermore, vertical
20 profiles of extensive and intensive optical properties referring to specific atmospheric
21 scenes for a set of selected scenarios are provided (i.e. Saharan dust, smoke from bi-
22 omass burning, ash from volcano eruptions, polar stratospheric clouds). The data used
23 for the development of LIVAS are presented in Section 2 while the methodologies
24 followed are given in Section 3. LIVAS product and its validation are presented in
25 Section 4, and the paper closes with our conclusions in Section 5.

1 **2. Data**

2 **2.1. The CALIPSO Level 2 product**

3

4 CALIOP, the principal instrument on board the CALIPSO satellite, part of the NASA
5 A-Train, is a standard dual-wavelength (532 and 1064 nm) backscatter lidar, operating
6 a polarization channel at 532 nm (Winker et al., 2009). CALIOP has been acquiring
7 high-resolution profiles of the attenuated backscatter of aerosols and clouds at 532
8 and 1064 nm along with polarized backscatter in the visible channel since 2006
9 (Winker et al., 2009). The horizontal resolution of CALIOP is 1/3 km while the verti-
10 cal resolution for the observations at 532 nm is 30 m from the surface to 8.3 km
11 height, 60 m from 8.3 to 20.2 km height, and 180 m from 20.2 to 30.1 km height. For
12 1064 nm it is 60 m from the surface to 20.2 km height and 180 m from 20.2 to 30.1
13 km height. This data is distributed as part of CALIPSO Level 1 product.

14 After calibration and range correction, cloud and aerosol layers are identified and aer-
15 osol backscatter and extinction at 532 and 1064 nm are retrieved as part of the Level 2
16 product. The product is produced by the application of a succession of algorithms that
17 are described in detail in a special issue of the Journal of Atmospheric and Oceanic
18 Technology (e.g., Winker et al., 2009). In brief, the CALIOP Level 2 retrieval scheme
19 is composed of feature detection and subtyping algorithms (modules that classify fea-
20 tures), and an extinction retrieval algorithm that estimates the aerosol backscatter and
21 extinction coefficient profile and total column aerosol optical depth (AOD) using an
22 assumed lidar ratio (LR) for each detected aerosol layer (the lidar ratio can be also
23 calculated in cases when clear air is available both above and below a layer (Young
24 and Vaughan, 2009)). The final CALIPSO Level 2 product includes the vertical loca-
25 tion of layers (Vaughan et al., 2009), the discrimination of aerosol layers from clouds
26 (Liu et al., 2009), the categorization of the aerosol layers in six subtypes (dust, ma-

1 rine, smoke, polluted dust, polluted continental, and clean continental; Omar et al.,
2 2009), and the AOD estimations for each layer detected (Young and Vaughan, 2009).
3 Due to CALIOP's sensitivity to polarization at 532 nm, the depolarization from non-
4 spherical dust particles serves as an independent means of discrimination between
5 dust and other aerosol species. In this study we used the Version 3 of the Level 2
6 product (Young and Vaughan, 2009).

7 **2.2. The EARLINET product**

8 EARLINET (<http://www.earlinet.org>) has been operating since 2000 aiming to estab-
9 lish a quantitative and comprehensive database for the aerosol vertical, spatial and
10 temporal distribution of aerosols on the European continental scale (Pappalardo et al.,
11 2014). To date, EARLINET includes 27 stations in 16 countries performing lidar ob-
12 servations on a regular schedule of one daytime measurement per week around noon
13 and two nighttime measurements per week with low background light in order to per-
14 form Raman extinction measurements (see Table 1 in Pappalardo et al., 2014). The
15 first volumes of the EARLINET database have been published in biannual volumes at
16 the World Data Center for Climate (The EARLINET publishing group 2000-2010,
17 2014 a, b). In addition to the routine measurements, further observations are devoted
18 to monitor special events such as Saharan dust outbreaks, forest fires and volcano
19 eruptions (The EARLINET publishing group 2000-2010, 2014 d, e). Moreover, since
20 14 June 2006 EARLINET has carried out collocated measurements with CALIPSO
21 during nearby overpasses, following a strategy defined on the basis of the ground-
22 track data analysis provided by NASA (Pappalardo et al., 2010; The EARLINET pub-
23 lishing group 2000-2010, 2014c).
24 EARLINET operation is coordinated such as to ensure instrument standardization and
25 consistent retrievals within the network. This harmonization is achieved through the

1 application of a rigorous quality-assurance program addressing both instrument per-
2 formance (Matthias et al., 2004; Freudenthaler et al., 2010) and evaluation of the algo-
3 rithms (Böckmann et al., 2004; Pappalardo et al., 2004).

4 The 14-year EARLINET database contains a large dataset of the aerosol lidar ratio
5 retrieved from simultaneous and independent lidar measurements of aerosol extinction
6 and backscatter coefficients. Moreover, this multi-wavelength database facilitates the
7 retrieval of extinction and backscatter spectral dependence for different aerosol types
8 after a proper layer identification and characterization. The lidar ratio is of fundamen-
9 tal importance for the estimation of aerosol extinction from pure backscatter lidar
10 measurements such as conducted by CALIOP, as well as the extinction and backscat-
11 ter spectral dependence is valuable for the spectral conversions between laser wave-
12 lengths.

13 **2.3. The AERONET product**

14 AERONET (<http://aeronet.gsfc.nasa.gov/>) is a global sunphotometric network with
15 more than 250 stations, employing the CIMEL CE318 photometer as the standard in-
16 strument (Holben et al., 1998). In AERONET, the calibration is centralized and
17 should be performed every 12 months, thus the instrument must be sent to specific
18 sites (in United States or Europe) for calibration and maintenance. AERONET meas-
19 urement schedule includes direct sun measurements at several wavelengths of the so-
20 lar spectrum (at 380, 440, 500, 675, 870, 1020 and 1640 nm depending on the instru-
21 ment type) as well as diffuse sky radiances at 440, 675, 870 and 1020 nm. Direct sun
22 measurements are used to retrieve the AOD at the measured wavelengths, the Ång-
23 ström exponent at 440/870 nm, and fine and coarse mode optical depth at 500 nm
24 (Holben et al, 2001; O'Neill, 2003). Direct sun and sky radiance measurements permit
25 the retrieval of the size distribution, the complex refractive index, and the Single-

1 Scattering Albedo (SSA) (Dubovik and King, 2000; Dubovik et al, 2000, Dubovik et
2 al. 2006).

3 **3. Methods**

4 In this section we describe the methods developed for the derivation of the multi-
5 wavelength LIVAS database. LIVAS was developed based on CALIPSO observations
6 at 532 and 1064 nm and includes the converted CALIPSO extinction and backscatter
7 product from 532 nm to 355, 1570 and 2050 nm (LIVAS wavelengths). For the spec-
8 tral conversion from CALIPSO 532 nm to the LIVAS wavelengths, we used aerosol-
9 type-dependent backscatter- and extinction-related Ångström exponents, as these were
10 derived from ground-based measurements or suitable optical models. Specifically, for
11 the conversions applied in LIVAS, the spectral dependence of the extinction and
12 backscatter was considered to follow the well-known Ångström exponential law as
13 follows:

$$14 \quad x_{par}(\lambda_2) = x_{par}(\lambda_1) \left(\frac{\lambda_1}{\lambda_2}\right)^{A_{\lambda_1/\lambda_2}} \quad (\text{Eq. 1})$$

15 where $x_{par}(\lambda_2)$ is the converted extinction or backscatter at λ_2 (either 355, 1570 or
16 2050 nm), A_{λ_1/λ_2} is the BAE or EAE and $x_{par}(\lambda_1)$ is the extinction or backscatter
17 product of CALIPSO at $\lambda_1=532$ nm. In the following, instead of extinction-related
18 Ångström exponents and backscatter-related Ångström exponents we use the terms
19 EAEs and BAEs respectively to describe the spectral dependence of the extinction
20 and backscatter.

21 An overview of the data and methods followed for the derivation of the aerosol-type-
22 dependent BAEs and EAEs is schematically illustrated in Figure 1 and described in
23 paragraph 3.1. The methodology for the spectral conversion of the CALIPSO Level 2
24 product is demonstrated through an example presented in paragraph 3.2. The section

1 closes with the description of the processing chain followed for quality filtering and
2 averaging the CALIPSO observations, given in paragraph 3.3.

3 **3.1. Derivation of spectral BAEs and EAEs**

4 For the derivation of the BAEs and EAEs we used different methods and datasets for
5 the UV and IR spectral regions: BAEs and EAEs for the 532 to 355 nm conversion
6 were mainly derived from the multi-wavelength EARLINET measurements of the
7 backscatter and extinction coefficients. EARLINET measurements cannot be used for
8 the IR conversion since the ground-based lidars of the network are spectrally limited
9 between 355 and 1064 nm. Thus, for converting the CALIPSO backscatter and extinc-
10 tion products from 532 nm to 1570 and 2050 nm, we first defined the typical size dis-
11 tributions and refractive indexes of the six aerosol subtypes used by CALIPSO (i.e.
12 dust, polluted dust, smoke, marine, clean continental and polluted continental, see also
13 Table 1 and detailed methodology in 3.1.2.) and then we calculated the respective
14 BAEs and EAEs utilizing well-known scattering codes like the Mie code for spherical
15 particles (Mie, 1908; Van de Hulst, 1957), as well as the T-matrix code (Mishchenko
16 et al., 2002) and the geometric-optics-integral-equation technique (Yang and Liou,
17 1996) for non-spherical particles.

18 The construction of representative size distributions and refractive indexes corre-
19 sponding to the CALIPSO aerosol types is not a straight-forward task. The ones used
20 to estimate the optical properties of each type in CALIPSO classification scheme, are
21 retrieved by clustering AERONET data in respective categories/aerosol types, as de-
22 scribed in Omar et al. (2005; 2009). Although this CALIPSO aerosol model is as-
23 sumed to correspond to the independently derived CALIPSO aerosol types, this is not
24 true for all cases, mainly due to the different nature of AERONET sunphotometer
25 measurements versus CALIPSO lidar measurements used for the categorization. The

1 main difference is that the sunphotometer is incapable of providing measurements at
2 the backscattering angle of 180° . For is the reason we did not use the CALIPSO aero-
3 sol model for the calculation of LIVAS BAEs and EAEs in the VIS-IR, and instead
4 we used different datasets and methods, as described in detail in section 3.1.2.

5 A different point that needs to be highlighted for LIVAS conversions is that the
6 CALIPSO classification used for the aerosol-type-dependent conversions possibly
7 introduces some uncertainty in LIVAS final product, due to inconsistencies with the
8 observed aerosol types. CALIPSO classification is based on a threshold algorithm that
9 takes into account the layer-integrated attenuated backscatter coefficient and an ap-
10 proximate particulate depolarization ratio as well as the surface type (either land or
11 ocean; Omar et al., 2009). However, these properties do not provide all the infor-
12 mation needed for unambiguously classifying the aerosol type and, as a result, mis-
13 classifications occur frequently (e.g. Burton et al., 2013). Since for LIVAS we need to
14 calculate BAEs and EAEs assuming that the CALIPSO aerosol types are representa-
15 tive of the aerosols observed, any inconsistencies in the CALIPSO classification
16 scheme introduce inaccuracies in our results.

17 Summarizing, LIVAS BAEs and EAEs were measured from EARLINET for the UV-
18 VIS conversion and they were calculated for the VIS-IR conversion. For the latter we
19 employed characteristic size distributions and refractive indexes from AERONET da-
20 ta classified into the respective aerosol types using different approaches, and further
21 validated using EARLINET measurements. Moreover, for aerosol types that are not
22 probed by either EARLINET or AERONET (e.g. marine), we utilized typical proper-
23 ties from the Optical Properties of Aerosols and Clouds (OPAC) model (Hess et al.,
24 1998) or other aerosol models from the literature. An elaborated description of our

1 methodology for the UV-VIS and VIS-IR spectral regions is given in paragraphs 3.1.1
2 and 3.1.2, respectively.

3 **3.1.1. BAEs and EAEs in UV-VIS spectral region**

4 For the conversion of CALIPSO aerosol backscatter and extinction from 532 to 355
5 nm, the aerosol-type-dependent BAEs and EAEs were derived from the EARLINET
6 database. Specifically, we used the database developed within the project “EAR-
7 LINET's Space-borne-related Activity during the CALIPSO mission” (ESA-
8 CALIPSO, Wandinger et al., 2011). ESA-CALIPSO is an ESA-funded study aimed to
9 establish an aerosol database from the classification of EARLINET observations per-
10 formed during nearby CALIPSO overpasses with respect to the aerosol type. The
11 methodology followed and the objectives of ESA-CALIPSO are described in
12 Wandinger et al. (2011). In brief, during ESA-CALIPSO a large number of
13 EARLINET observations was utilized to develop an aerosol classification scheme
14 over Europe and to determine the respective type-dependent BAEs and EAEs, togeth-
15 er with other aerosol intensive properties. Each EARLINET measurement was in-
16 spected regarding quality (e.g., noise level) and the occurrence of distinct aerosol lay-
17 ers. For each selected layer, an air-mass transport simulation was performed to deter-
18 mine its origin, transport path, and age. Additional modeling tools and satellite prod-
19 ucts (e.g., fire maps) were implemented to cross-check the sources and to assign an
20 aerosol type for each layer (Wandinger et al., 2011).

21 For the derivation of the UV-VIS (355 from 532 nm) BAEs and EAEs in LIVAS, we
22 used the measurements from more than 500 aerosol layers recorded in the ESA-
23 CALIPSO database and provided by four high-performance EARLINET stations,
24 namely the stations of Athens, Leipzig, Potenza and Thessaloniki. The final BAEs and
25 EAEs were calculated by averaging the measurements collected for each aerosol type.

1 These are presented in the left column of Table 2 for backscatter (bsc) and extinction
2 (ext).

3 The EARLINET measurements included in ESA-CALIPSO regarding clean marine,
4 clean continental and stratospheric aerosol particles were limited for a reliable statisti-
5 cal analysis. The calculation of BAEs was possible, but for EAEs this was not the case
6 (mainly due to Raman lidar constraints regarding the overlap that prohibits extinction
7 retrievals for lower marine atmospheric layers and regarding inadequate Raman re-
8 turns from the stratosphere). For the aforementioned types, aerosol models provided
9 in the literature were used in order to calculate the EAEs. Specifically, we used the
10 maritime model introduced in Sayer et al. (2012) for clean marine aerosols, the OPAC
11 model for clean continental aerosols and the stratospheric model of Wandinger et al.
12 (1995) and Deshler et al. (1993) for stratospheric aerosols. From these models, typical
13 size distributions and refractive indexes were retrieved and the BAEs and EAEs were
14 calculated via the application of the Mie theory (Mie, 1908; Van de Hulst, 1957). The
15 results are provided in Table 2 (left column).

16 **3.1.2. BAEs and EAEs in VIS-IR spectral region**

17 ESA-CALIPSO is mainly limited to the VIS-UV spectral region. For the VIS-IR con-
18 versions in LIVAS, we used typical size distributions and refractive indexes for each
19 aerosol type derived from AERONET data or models, i.e. OPAC or other aerosol
20 models in the literature. Scattering simulations were then applied for each aerosol type
21 for the complete spectral range of LIVAS interest (i.e. 355, 532, 1064, 1570, 2050
22 nm). The criterion for selecting between different approaches for each aerosol type
23 was the consistency of the calculations in the UV-VIS spectral region with the ESA-
24 CALIPSO measurements, which were the reference for any conversion made in
25 LIVAS. More specifically, we checked the consistency of our calculations with ESA-

1 CALIPSO for the 532-to-355-nm EAEs and the 532-to-355-nm, 355-to-1064-nm and
2 532-to-1064-nm BAEs.

3 The different approaches for the derivation of the typical microphysical properties in
4 LIVAS aerosol model are described in the following:

5 AERONET-Omar: AERONET data were categorized with respect to the CALIPSO
6 aerosol types based on the classification method introduced by Omar et al. (2005;
7 2009), utilized for the construction of the CALIPSO aerosol model as described
8 above. The difference in our approach for the LIVAS aerosol model was that for each
9 aerosol type a consistency check with the ESA-CALIPSO data was first performed:
10 each AERONET measurement was categorized under a specific aerosol type and the
11 Ångström exponent at 355/532 nm and the lidar ratios at 355 and 532 nm were com-
12 puted (using the phase function and the SSA provided by AERONET). Then, we re-
13 jected the cases for which the aforementioned calculated optical properties were not
14 within the range of the typical ESA-CALIPSO values for the respective aerosol type.
15 From the constrained dataset, the average size distribution and refractive index were
16 produced for each aerosol type and subsequently used as input in scattering calcula-
17 tions to produce the spectral BAEs and EAEs in the VIS-IR spectral range. The meth-
18 od was expected to derive consistent microphysics with ESA-CALIPSO at the UV-
19 VIS range and thus the results for the VIS-IR spectral range would be consistent.

20 For the scattering calculations the well-known Mie code (Mie, 1908; Van de Hulst,
21 1957) was applied for all the aerosol types except the non-spherical particles of dust
22 and polluted dust, where the T-matrix code and the geometric-optics-integral-equation
23 technique were utilized instead. More specifically, for the non-spherical scattering
24 calculations we employed the code of Dubovik et al. (2006), which utilizes the T-
25 matrix method for particles of size parameter $\left(\frac{2 \times \pi \times \text{radius}}{\text{wavelength}}\right)$ smaller than 20-30 and the

1 geometric-optics-integral-equation technique for larger particles, with size parameter
2 up to ~ 625 . The non-spherical particles were considered as mixtures of spheroids with
3 aspect ratios defined by an aspect-ratio distribution, and pre-computed look-up tables
4 were utilized, allowing fast calculations. We considered that the non-spherical parti-
5 cles of dust and polluted dust over their entire size range have the same aspect ratio
6 distribution as the one provided for dust in Dubovik et al. (2006), which was shown to
7 reproduce successfully the laboratory measurements of mineral dust scattering proper-
8 ties by Volten et al. (2001).

9 AERONET-CALIPSO: AERONET and CALIPSO collocated and synchronized
10 measurements were collected, following the collocation method introduced in Schus-
11 ter et al. (2012). More specifically, the spatial collocation required the CALIPSO
12 overpass to be closer than 80 km from the AERONET station and the measurements
13 to take place with maximum 30 min difference. From the collocated measurements,
14 only those with a single CALIPSO aerosol subtype in the atmospheric column were
15 considered. The AERONET data for these cases were subsequently classified based
16 on the aerosol type provided by the collocated CALIPSO measurements. Scattering
17 calculations were applied to each of the AERONET size distributions and refractive
18 indexes of the collected cases taking into account the spherical and non-spherical part
19 of the mixture, as this was provided by AERONET for each case.

20 It should be highlighted here that for this method there was no distinction between
21 spherical and non-spherical aerosol types, instead all types were considered to contain
22 both spherical and non-spherical particles, in accordance with the AERONET prod-
23 uct. The calculations for the spherical part were performed with the Mie code and for
24 the non-spherical part with the Dubovik et al. (2006) code, following the methodology

1 described above. For each type, all the collocated cases were averaged and from those
2 measurements we derived the average values of BAEs and EAEs.

3 The dataset was not constrained with ESA-CALIPSO as in the AERONET-Omar ap-
4 proach for the UV-VIS wavelengths. This was due to the fact that the specific ap-
5 proach aimed to deliver typical BAEs and EAEs for the aerosol types classified by the
6 CALIPSO classification scheme itself, thus no correspondence to the nature of the
7 atmospheric aerosol loads was required.

8 OPAC: A typical size distribution and refractive index were extracted from the OPAC
9 dataset for the clean continental type, considering typical ambient conditions of 70%
10 relative humidity. We derived the BAEs and EAEs by performing scattering calcula-
11 tions with the Mie code. Since for the clean continental aerosol there is little to no in-
12 formation from AERONET and EARLINET we had to rely on models to derive
13 LIVAS BAEs and EAEs.

14 Approaches taken from the literature: The studies of Wandinger et al. (1995) and
15 Deshler et al. (1993) provide a range of typical size distributions and refractive index-
16 es for the stratospheric aerosol, while the maritime model of Sayer et al. (2012) pro-
17 vides a typical size distribution and refractive index for marine aerosol. We derived
18 the corresponding BAEs and EAEs by performing scattering calculations with the Mie
19 code.

20 **3.1.3. Final LIVAS BAEs and EAEs per aerosol type and evaluation against** 21 **ESA-CALIPSO database**

22 As already mentioned, LIVAS BAEs and EAEs need to be consistent with ESA-
23 CALIPSO, a reference database of measured lidar-related aerosol properties. While
24 the UV-VIS BAEs and EAEs were derived directly from the ESA-CALIPSO data-
25 base, the VIS-IR BAEs and EAEs were calculated using the datasets and methods de-

1 scribed in section 3.1.2. To ensure consistency of our calculations with measured data,
2 for each aerosol type we selected the VIS-IR methodology that provided compatible
3 results with the ESA-CALIPSO for the UV-VIS BAEs and EAEs. In this way we en-
4 sured the best possible consistency of BAEs and EAEs for the entire spectral range.
5 Our final results are presented and discussed herein: Figure 2 shows the calculated
6 BAEs and EAEs using all the approaches described in section 3.1.2 and their compar-
7 ison with ESA-CALIPSO at UV-VIS. The selected approach for each aerosol type is
8 denoted in Figure 2 with large size symbols. Starting from the AERONET-Omar ap-
9 proach, we found that it performed better when compared to ESA-CALIPSO for the
10 polluted continental type, resulting in a very good agreement for the EAE and best
11 performance regarding the BAEs. For the other types this approach reproduced well
12 the EAEs but the BAEs could not be reproduced such as to fit the ESA-CALIPSO ac-
13 ceptable range of values. Dust and polluted dust aerosols are most likely classified
14 correctly by CALIPSO due to its polarization sensitivity (e.g. Burton et al., 2013;
15 Amiridis et al., 2013). For this reason, we chose the AERONET-CALIPSO approach
16 for the calculation of their BAEs and EAEs. The approach showed a relatively better
17 agreement with ESA-CALIPSO compared to the AERONET-Omar approach, espe-
18 cially for the BAEs, maybe due to better filtering of the AERONET data used in the
19 calculations for the AERONET-CALIPSO approach (Figure 2). Overall though, we
20 believe that the discrepancies in backscatter spectral dependence observed for most of
21 the aerosol types are most likely due to the fact that AERONET lacks the capability to
22 directly measure in the backscattering direction. Comparisons found in the literature
23 between Raman-lidar-measured and photometer-retrieved lidar ratios, support this ar-
24 gument (e.g. Mueller et al., 2007).

1 Moreover, it should be noted that the evaluation of the retrieved values with ESA-
2 CALIPSO for polluted dust is only indicative. This is because CALIPSO assumes the
3 same properties for any kind of dust mixture (e.g. dust-smoke, dust-marine) while
4 ESA-CALIPSO shows that the optical properties are highly variable for different dust
5 mixtures. Specifically, ESA-CALIPSO provides intensive properties for mixtures of
6 dust with polluted continental, smoke and marine aerosol separately and what we used
7 here in order to compare with CALIPSO is an average of these properties.

8 For smoke aerosols the AERONET-CALIPSO approach showed similar results as
9 AERONET-Omar, performing well for EAE, but failing to reproduce the ESA-
10 CALIPSO BAEs (Figure 2). For this aerosol type we used the calculated BAEs and
11 EAEs from the AERONET-CALIPSO approach for LIVAS conversions. This deci-
12 sion was based on the fact that the classification of smoke by CALIPSO is the most
13 uncertain compared to the other aerosol types, as reported by Burton et al. (2013). The
14 authors of this study reported a percentage agreement of 13% for smoke classification
15 when comparing with airborne HSRL classification results. Smoke misclassification
16 was also found to be the reason of the discrepancies between CALIPSO and
17 AERONET reported in Schuster et al. (2012) in terms of AOD measurements. These
18 findings indicate that the CALIPSO smoke classification may not correspond to real
19 smoke presence. Thus, it may not be comparable with real smoke detections by
20 EARLINET in ESA-CALIPSO. This is because the ESA-CALIPSO classification
21 model is based on source-receptor analysis based on model simulations of air mass
22 advection over the stations, together with the aerosol optical properties measured by
23 the lidar. Thus, for the smoke type we avoided to use the ESA-CALIPSO smoke sta-
24 tistics.

1 For clean marine and clean continental aerosol, the ESA-CALIPSO database does not
2 contain an adequate number of measurements to provide statistically significant aver-
3 ages. Thus, for clean marine we used the size distribution and refractive index provid-
4 ed in the maritime model of Sayer et al. (2012) and for clean continental we used the
5 ones provided in the OPAC database. Note that the size distribution and refractive in-
6 dex for clean continental aerosol from OPAC database were considered at ambient
7 conditions of 70% relative humidity.

8 Finally, for the stratospheric aerosol type we used the model introduced in Deshler et
9 al. (1993) and Wandinger et al. (1995). BAEs and EAEs found to be in good agree-
10 ment with ESA-CALIPSO values (not shown in Figure 2).

11 The final aerosol-type-dependent VIS-IR BAEs and EAEs used in LIVAS are pre-
12 sented in the right panel of Table 2 for extinction (ext) and backscatter (bsc). Overall,
13 as seen in Figure 2, LIVAS is compatible with ESA-CALIPSO in the VIS-UV spec-
14 tral region regarding EAEs. However, the agreement with regard to the VIS-UV
15 BAEs is not that satisfactory. For the BAEs and EAEs in the IR, one point of concern
16 is the extrapolation of the refractive index at the longer wavelengths, since this infor-
17 mation is not provided from AERONET.

18 **3.1.4. Comparison of LIVAS and CALIPSO aerosol models**

19 The microphysical properties used for calculating the VIS-IR BAEs and EAEs are
20 compared in this section with the ones of CALIPSO aerosol model (Omar et al. 2005;
21 2009). Figure 3 shows the comparison of LIVAS versus CALIPSO size distributions
22 for each aerosol type, while Figure 4, 5 and 6 show the spectral dependence of the
23 complex refractive index and the SSA, respectively, at LIVAS wavelengths for the
24 two models. Figure 7 shows the BAE and EAE at 355/532 nm, the lidar ratio at 532
25 nm and the effective radius for the LIVAS and CALIPSO aerosol models, compared

1 with the ones provided in the ESA-CALIPSO database. The values of the lidar ratio at
2 532 nm, the SSA at 532 nm and the effective radius for the two models are also pro-
3 vided in Table 3.

4 In Figure 3 the best agreement between the LIVAS and the CALIPSO model size dis-
5 tributions is found for the polluted continental type. For smoke particles the
6 CALIPSO model considers the same volume for fine and coarse particles, whereas the
7 LIVAS model presents a domination of the fine mode. The latter agrees well with the
8 averaged size distribution of smoke type provided in Dubovik et al. (2002)
9 AERONET eight-year climatology and is considered more typical as it is supported
10 by other studies as well as (Reid et al., 2005; Eck et al., 1999; 2003). For dust type the
11 LIVAS size distribution has fewer fine particles than the CALIPSO model, in agree-
12 ment with the AERONET climatology of Dubovik et al. (2002) and findings of exper-
13 imental campaigns dedicated to mineral dust characterization (e.g. McConnell et al.,
14 2008; Weinzierl et al., 2009; Müller et al., 2011; Toledano et al., 2011). For the pol-
15 luted dust type both models seem to fall within the range of the large variability re-
16 ported in the literature for dusty mixtures (Eck et al., 1999; Jung et al., 2010). The
17 more pronounced fine mode in the LIVAS model resembles the size distributions of
18 dust and pollution mixtures (Kim et al., 2007). However, an extensive discussion on
19 the polluted dust type is avoided here since there is no clear definition of the non-dust
20 components for this type in the CALIPSO model. LIVAS size distribution for clean
21 marine type is based on the maritime model of Sayer et al. (2012). Similar size distri-
22 butions for marine particles are provided in other studies as well (e.g. Dubovik et al.,
23 2002; Smirnov et al., 2002). The largest disagreement is seen for the clean continental
24 type. We believe that the pronounced fine mode in the LIVAS size distribution from
25 OPAC is due to the hygroscopic growth of the hydrophilic fine particles in ambient

1 relative humidity of 70%. However, the clean continental type in global CALIPSO
2 records has a contribution of the order of 2%, making this type of less importance for
3 LIVAS database. For the aerosol model though, a better definition of the aerosol
4 components of this type should be considered.

5 Regarding the differences on the refractive index assumed by LIVAS and CALIPSO
6 aerosol models, these are presented in Figures 4 and 5, respectively, for the reader's
7 reference. We also present a comparison of the LIVAS and CALIPSO SSA in Figure
8 6. The comparison shows an overall disagreement in the SSA for the two aerosol
9 models. We should note here that Omar et al. (2009) provide the refractive index val-
10 ues at 532 and 1064 nm and we used linear extrapolation to estimate the CALIPSO
11 refractive indexes for the other wavelengths of LIVAS (see Figures 4 and 5). Despite
12 the disagreement of the SSA values, their spectral slope is similar for all the types
13 (except the clean continental aerosol) for both models. Even more so, for polluted
14 continental, dust, smoke and clean marine particles the spectral slope of the SSA
15 agrees relatively well with the corresponding ones provided in Dubovik et al. (2002)
16 climatology. More specifically, for the dust type the spectral slope of the SSA for both
17 models is flatter but it closely resembles the one presented in Dubovik et al. (2002), as
18 well as in other studies (Müller et al., 2011; Toledano et al., 2011). For smoke, the
19 absorption has to do mainly with the black carbon content and can greatly vary (Eck
20 et al., 2003). The spectral dependence and range of LIVAS SSA values are similar
21 with the values provided in Dubovik et al. (2002) climatology and references therein,
22 whereas the CALIPSO SSA have lower values, which although agree with other stud-
23 ies (e.g. Eck et al., 1998; 2003). The polluted dust SSA spectral dependence is similar
24 for both models, but different than of dust mixtures with smoke and pollution present-
25 ed in the literature (e.g. Jung et al., 2010; Holler et al., 2003). Finally, the clean ma-

1 rine SSA for both models agrees very well with other studies in the literature (e.g.
2 Dubovik et al, 2002; Hasekamp et al., 2011).

3 In Figure 7, a final comparison between ESA-CALIPSO, LIVAS and CALIPSO is
4 given in terms of BAE and EAE, lidar ratio at 532 nm and effective radius. BAE and
5 EAE at 355/532 nm are not provided by Omar et al. (2009) and instead they were cal-
6 culated using the size distribution and refractive index of the CALIPSO model. For
7 the scattering calculations we used the Mie code for the types with spherical particles
8 and the Dubovik software for the non-spherical particles of dust and polluted dust
9 types. The methodology was the same as the one described for the AERONET-Omar
10 approach in Section 3.1.2. The lidar ratio at 532 nm was taken directly from what is
11 reported in Omar et al. (2009), while due to the fact that the effective radius is not
12 given in this work, it was calculated from the size distribution for each type therein.

13 We need to highlight here that our focus is evaluating LIVAS BAEs and EAEs con-
14 sistency with the ESA-CALIPSO measurements. The lidar ratio and effective radius
15 are not used in generating LIVAS database and are only provided here for reasons of
16 completeness. We should make a comment though about the large LIVAS dust lidar
17 ratio, which we believe is an artefact due to the aspect ratio distribution used in the
18 non-spherical particle scattering calculations. As shown in the recent paper of Koepke
19 et al. (2015), in order to reproduce successfully the dust optical properties, the aspect
20 ratio distribution needs to change with particle size. This is something that indicates
21 that more work is needed to develop an aerosol model oriented for space-borne lidar
22 applications.

23 Concerning the BAE and EAE at 532 nm, the maximum deviation is found for BAE,
24 whereas for EAE we get an overall agreement between LIVAS, CALIPSO and ESA-
25 CALIPSO. The deviation in LIVAS and CALIPSO BAE is especially evident for the

1 dust type (Figure 7 upper-right), possibly due to the lower effective radius produced
2 from the large fine-mode contribution in the size distribution assumed in Omar et al.
3 (2009). For polluted continental aerosol we get a relatively good agreement for
4 LIVAS and ESA-CALIPSO BAEs, but this is not the case for the CALIPSO BAE.
5 For smoke aerosol the LIVAS and CALIPSO agreement is good, but there is no con-
6 sistency with ESA-CALIPSO. For clean marine aerosol all three BAEs agree well.
7 For clean continental LIVAS BAE agrees with ESA-CALIPSO, but CALIPSO BAE
8 is quite different. Overall, we find that the LIVAS BAEs are closer to the ESA-
9 CALIPSO measured values than the CALIPSO BAEs.

10 **3.1.5. Spectral conversions for other LIVAS products**

11 Depolarization spectral conversions were not applied in LIVAS since multi-
12 wavelength depolarization measurements are rare and available only during experi-
13 mental campaigns (Freudenthaler et al., 2009; Groß et al., 2011a, b), thus the dataset
14 was not considered statistically significant. A single-wavelength depolarization data-
15 base is provided in LIVAS using CALIPSO Level 2 particle depolarization ratio aver-
16 ages at 532 nm.

17 Furthermore, a global cloud database is given based on CALIPSO observations at 532
18 nm. With respect to clouds, the wavelength conversion is most probably of minor im-
19 portance due to approximately neutral scattering behavior along the range of LIVAS
20 wavelengths.

21 In addition, a database for the stratospheric features detected by CALIPSO is provid-
22 ed, separated to cloud and aerosol features. Specifically, the stratospheric features de-
23 tected by CALIPSO were separated in polar stratospheric clouds and stratospheric
24 aerosols using the temperature threshold technique proposed by Pitts et al. (2009). In
25 brief, we classified the stratospheric features as Polar Stratospheric Clouds (PSCs) for

1 temperature lower than 198 K, while features of higher temperatures were classified
2 as stratospheric aerosols. The separation was applied only for stratospheric features at
3 latitudes greater than 54° N and less than -54°S, while for the latitudes in between, the
4 stratospheric features were considered as aerosols. This classification is not consid-
5 ered reliable enough and has been included in LIVAS in order to provide only a rough
6 estimate of the stratospheric aerosol loads detected by CALIPSO. More efforts will be
7 needed in the future for achieving a trustworthy separation of different stratospheric
8 features. As proposed by Pitts et al. (2009), the utilization of L1 CALIPSO product in
9 synergy with L2 may provide a more reliable discrimination.

10 Finally, a set of selected scenes of specific atmospheric phenomena (e.g. dust out-
11 breaks, volcanic eruptions, wild fires, polar stratospheric clouds) was produced. BAEs
12 and EAEs for the selected scenes were delivered after thorough investigation of each
13 case study, based on CALIPSO-collocated ground-based measurements that are re-
14 ported in the literature. Whenever this was not possible (as for the IR conversion), the
15 LIVAS BAEs and EAEs were used.

16 **3.2. Example for the spectral conversion of single CALIPSO profiles**

17 The obtained aerosol-type-dependent BAEs and EAEs for UV-VIS and VIS-IR were
18 applied to the CALIPSO Level 2 product at 532 nm for the respective aerosol layer
19 type inferred by the CALIPSO aerosol classification scheme. An example of the con-
20 version from 532 to 355 nm is presented in Figure 8. Each CALIPSO layer in the pro-
21 file example was converted from 532 to 355 nm using the LIVAS EAE at 355/532,
22 depending on the aerosol type retrieved by the CALIPSO aerosol classification
23 scheme for the layer. In the example presented in Figure 8, LIVAS EAEs for clean
24 marine (0.78), dust (0.55) and polluted continental (1.24) types were applied to the

1 CALIPSO extinction coefficient at 532 nm, based on the Ångström exponential law
2 described in Equation 1.

3 **3.3. CALIPSO quality filtering and averaging processing chain**

4 For the production of the final LIVAS products, we used the methodology developed
5 by the CALIPSO team for the Level 3 aerosol product, as described in Winker et al.
6 (2013). Our algorithm was tested for reproducing the CALIPSO Level 3 product,
7 which is an aggregation onto a global 2x5 degree latitude-longitude grid. After the
8 positive evaluation of the averaging procedure (not shown here), we applied it on the
9 Level 2 CALIPSO profiles at 532 and 1064 nm but also on the corresponding LIVAS
10 spectrally converted profiles at 355, 1570 and 2050 nm, in order to derive 1x1 degree
11 latitude-longitude averaged vertical distributions. The vertical resolution of the
12 LIVAS product is identical to CALIPSO Level 3, namely 60 m in the tropospheric
13 region between the surface and 20 km and 180 m in the stratospheric region between
14 20 and 30 km.

15 As input to the averaging algorithm, we used the Version 3 CALIOP Level 2 aerosol
16 profile product, applying quality screening prior to averaging, to eliminate samples
17 and layers that were detected or classified with very low confidence, or that contained
18 untrustworthy extinction retrievals. In brief, the filters concerned the: Cloud-Aerosol
19 Discrimination (CAD) score, Extinction Quality Control (QC) flag, aerosol extinction
20 uncertainty, isolated 80 km layer, misclassified cirrus, undetected surface attached
21 aerosol low bias, large negative near-surface extinction, surface contamination be-
22 neath surface-attached opaque layer, removal of samples below opaque cloud and
23 aerosol layers. Detailed explanation of the methodology followed for the production
24 of the Level 3 product and respective filtering and flags, is provided in the Appendix
25 of Winker et al. (2013). For the particle linear depolarization, an extra filter was ap-

1 plied in LIVAS in order to average this parameter for the same samples collected for
2 the extinction. For that, we averaged only the particle linear depolarization CALIPSO
3 retrievals for which the extinction uncertainty is less than 99.9 km^{-1} , so as to maintain
4 the same measurement sampling. For the quality screening of cloud and stratospheric
5 feature profiles a similar methodology was followed.

6 In the CALIPSO Level 3 product, four types of products were generated each month,
7 depending on sky condition and temporal coverage, and were separated into day/night
8 segments. In LIVAS, only the “combined” product was used (Winker et al. 2014) in
9 order to achieve better quality of the aerosol dataset regarding cloud discrimination
10 and measurement accuracy. Moreover, beyond the mean extinction profiles for the
11 total aerosol load, LIVAS provides mean extinction profiles at 532 nm for each of the
12 six aerosol types in the CALIPSO classification scheme. Finally, the seasonal distri-
13 bution of the vertical distribution of the extinction for each LIVAS cell is also provid-
14 ed. A schematic outline of the LIVAS processing chain is given in Figure 9.

15 **4. Results and discussion**

16 **4.1. LIVAS products**

17 The final LIVAS aerosol/cloud database contains multi-wavelength 4-year averaged
18 vertical distributions and statistics for a global grid of 1x1 degree. Here, we demon-
19 strate the LIVAS products through an example for one grid cell corresponding to our
20 hometown, Athens, in Greece (centroid latitude of 38.5° North and longitude of 23.5°
21 East).

22 In the upper panel of Figure 10 the aerosol extinction is given for the LIVAS lidar
23 wavelengths, i.e. 355, 532, 1064, 1570, 2050 nm, along with the standard deviation of
24 the averaging at 532 nm (grey line). The number of observations is presented in the
25 right panel for each plot, in order to have a measure of the representativeness of the

1 mean aerosol extinction for each cell, which depends on the available CALIPSO
2 overpasses and corresponding samples. The maximum surface elevation over the
3 CALIPSO overpass is given for the grid cell of interest, as obtained from the digital
4 elevation map (DEM) used by CALIPSO. In the middle panel of Figure 10, the mean
5 extinction profile is given per CALIPSO aerosol type, while in the lower panel the
6 mean extinction is given per season with the corresponding sampling/occurrences
7 used for their production.

8 Additional LIVAS products are provided for particle depolarization at 532 nm. These
9 refer to the mean particle depolarization along with its standard deviation (Figure 11 –
10 upper panel). Moreover, mean cloud extinction at 532 nm is given in LIVAS (Figure
11 11 – middle panel) along with mean extinction coefficient of stratospheric features in
12 total (Figure 11 – lower panel) but also for PSCs and aerosol particles separately.

13 Finally, for each grid cell a number of statistical parameters are provided in LIVAS
14 regarding the mean, minimum and maximum surface elevation, the number of over-
15 passes for each cell, the number of examined profiles, the samples averaged after fil-
16 tering (total, aerosol, clear air), the subtype occurrence in the aerosol total observa-
17 tions (in percentages) and the AOD at 532 nm (mean, median and standard deviation).

18 **4.2 LIVAS AOD evaluation**

19 In this section an evaluation of the LIVAS climatological AOD mean values at 532
20 nm is given, using collocated AERONET AOD averages. AERONET stations includ-
21 ed in each grid cell of 1x1 degree were considered representative when the stations
22 were operated for the same time period with LIVAS (2008-2011). LIVAS mean AOD
23 was calculated by the integration of the 4-year-averaged extinction profile, while
24 AERONET AOD was calculated by averaging all available station data. A first com-
25 parison of LIVAS AODs against AERONET is presented in Figure 12. Blue circles

1 denote the absolute value of the difference (LIVAS mean AOD – AERONET mean
2 AOD), while the red crosses denote the elevation difference between the AERONET
3 site and the mean elevation of the CALIPSO ground track. This map provides only the
4 magnitude of biases (absolute values) to demonstrate the range of discrepancies with
5 respect to the elevation slope. Large differences can also be attributed to specific grid
6 cell under-sampling by CALIPSO in the 4-year period, as discussed below.

7 Large elevation differences may cause large AOD biases since in such cases the opti-
8 cal path lengths monitored by AERONET and CALIPSO instruments can vary.
9 Moreover, when CALIPSO overpasses high-slope terrains, the sampling may become
10 inadequate for heights lower than the maximum elevation. An example of such a case
11 is given in Figure 13 for the AERONET station of “ND_Marbel_Univ” in Philippines.
12 CALIPSO overpasses this station over elevations ranging from zero to 1.46 km. The
13 number of observations for heights lower than the maximum elevation becomes very
14 small (Figure 13 – right panel) and inadequate for statistical purposes. This under-
15 sampling affected the final averaged extinction profile as shown in the left panel of
16 Figure 13 for heights lower than the maximum elevation. In order to eliminate these
17 effects from the comparison of LIVAS with AERONET, we applied on our dataset
18 the following constraints:

- 19 1) The elevation difference between the AERONET site and CALIPSO mean ground
20 track elevation was kept below 100 m.
- 21 2) The elevation slope in CALIPSO overpass was constrained to be less than 400 m.
- 22 3) CALIPSO sampling was controlled by constraining the comparison over grid cells
23 with large number of overpasses, i.e. over 150.

24 The third constraint is considered crucial for the representativeness of LIVAS data-
25 base. As shown in Figure 14, in approximately 30% of the global 1x1 degree cells of

1 the database the number of overpasses is less than 150. This under-sampling along
2 with possible high-slope terrains could cause unrealistic results.

3 Figure 15 presents the absolute bias of the means for our constrained dataset (i.e.
4 LIVAS mean AOD – AERONET mean AOD). For most sites the comparison reveals
5 biases within ± 0.1 in terms of AOD. Negative LIVAS biases lower than -0.1 (denoted
6 in Figure 15 with blue color) are found mostly over the Saharan desert, a result that
7 may be related to possible CALIPSO underestimations for dust as already reported in
8 the literature (e.g. Wandinger et al., 2010; Schuster et al., 2012; Tesche et al., 2013;
9 Amiridis et al., 2013). Positive LIVAS biases larger than 0.1 denoted with red color in
10 Figure 15 are mostly found over coastlines. This effect is not well understood yet.
11 Campbell et al. (2012) found CALIPSO offsets over coastlines when comparing with
12 the U.S. Naval Aerosol Analysis and Predictive System (NAAPS). Recently, Kanitz et
13 al. (2014) found a systematic overestimation of the AOD over land in coastal areas of
14 up to a factor of 3.5. The researchers attributed the possible CALIPSO overestimation
15 to the surface-dependent criterion (land/ocean) included in the classification scheme
16 which may prohibit a correct classification of sea-breeze-related marine aerosol over
17 land, leading to unrealistically high lidar ratio assumptions.

18 We have to mention here that the LIVAS validation presented in Figure 15 cannot be
19 conclusive on the aforementioned possible issues. Overall, the global LIVAS agree-
20 ment with AERONET within 0.1 AOD is considered a very good result for a 4-year
21 product. Keeping the constrained dataset for a quantitative comparison, we present in
22 Figure 16 scatter plots for AOD averages at the different LIVAS wavelengths. In the
23 upper panel we show the comparison for the averaged AOD at 532 nm (left) and for
24 the standard deviation of the distribution (right). A Pearson correlation coefficient of
25 0.86 reveals a very good agreement for the AOD at 532 nm. The slope of the linear

1 regression is 0.79, showing a slight underestimation of the LIVAS AOD. Since the
2 532 nm LIVAS products come directly from CALIPSO averages, this underestimation
3 is probably related to CALIPSO limitations (e.g. Schuster et al., 2012; Omar et al.,
4 2013). The variability of the CALIPSO samples averaged for LIVAS is consistent
5 with AERONET as shown in the upper right panel of Figure 16. The LIVAS AOD at
6 355 nm (lower left panel) is also in a very good agreement with AERONET, showing
7 similar values of Pearson's r and slope as those of the 532 nm comparison. This result
8 shows that the conversion of the CALIPSO extinction product from 532 to 355 nm
9 using the EARLINET BAEs and EAEs is successful. Regarding the comparison at IR
10 wavelengths (lower right panel), the results are not encouraging. LIVAS AOD at 1570
11 nm is consistent with AERONET for AODs lower than 0.1 but not for higher values
12 where LIVAS heavily underestimates. This can be attributed to errors introduced due
13 to the extrapolation of the AERONET AOD in the IR (note that we used AERONET
14 AOD measurements at 440, 670, 860 and 1020 nm), and/or to uncertainties introduced
15 by the LIVAS conversion scheme in the IR.

16 **4.3 LIVAS web-portal**

17 The LIVAS database is freely available under the url:
18 <http://lidar.space.noa.gr:8080/livas/>, where the database is stored and exposed (Figure
19 17). The webpage provides the complete information on the methodological ap-
20 proaches and instructions on portal's usage. The data are provided in ASCII and
21 netcdf formats, while brief statistics and quick-view charts are projected online. The
22 user can select to download the database via ftp, or navigate to the region of interest
23 by using a dynamic map to select over the World grid of 1x1 degree spatial resolution.
24 The map provides the possibility to overlay a layer that represents the number of
25 CALIPSO overpasses. This is considered crucial for the use of the database since only

1 grid cells with a number of CALIPSO overpasses greater than 150 are recommended
2 for their statistical representativeness. Moreover, the user can overlay global AODs or
3 cloud optical depths on the map. In the example of Figure 18, the global distribution
4 of LIVAS AODs is presented, showing high values over well-known sources like the
5 dust belt, India and China as well as transport paths as the one from Sahara westward
6 across the Atlantic.

7 **5. Summary and conclusions**

8 We presented LIVAS, a 4-year multi-wavelength global aerosol and cloud optical da-
9 tabase that has been developed for complementing existing datasets used by ESA for
10 instrument performance simulation of current and future space-borne lidars as well as
11 retrieval algorithm testing activities based on realistic atmospheric scenarios. In order
12 to cover the different spectral domains for HSRL and IPDA lidars, the compiled data-
13 base addresses the three harmonic operating wavelengths of Nd-YAG lasers (355, 532
14 and 1064 nm) as well as typical wavelengths of IPDA lidars in the SWIR spectral
15 domain (1570 and 2050 nm).

16 When compared to AERONET, the LIVAS AOD values appeared to be realistic and
17 representative for VIS wavelengths but also for UV, making this database appropriate
18 for use by ADM-Aeolus and EarthCARE. Regarding the IR conversion however,
19 LIVAS is not considered representative when compared to AERONET, especially for
20 AODs higher than 0.1. We believe that LIVAS is representative in the UV due to the
21 fact that the UV-VIS BAEs and EAEs were provided by ground-based lidar meas-
22 urements of high quality as those provided by EARLINET. Moreover, the methodolo-
23 gy used for the application of the conversions was based on aerosol classification ad-
24 vances developed within the ESA-CALIPSO project. For IR however, the BAEs and
25 EAEs were not measured but instead retrieved from scattering simulations using typi-

1 cal size distributions and refractive indexes assumed for each CALIPSO aerosol type,
2 deduced from AERONET data and aerosol models provided in the literature. Even
3 though EARLINET was used to constrain the IR simulations, the final results were
4 not satisfactory and more work is needed that would benefit from potential future IR
5 ground-based measurements. However, LIVAS BEAs and EAEs were found to be
6 more consistent with ESA-CALIPSO but also with the relative literature than the one
7 used by CALIPSO.

8 In the future, we plan to expand LIVAS in monthly-averaged aggregations in order to
9 provide timeseries for UV lidar products. In this way, LIVAS timeseries could be ho-
10 mogenized in the future with EarthCARE products for the consolidation of a multi-
11 year aerosol/cloud multi-wavelength 4D dataset appropriate for climate studies. How-
12 ever, the challenges for this task are significant, due to a number of open scientific
13 questions and related knowledge gaps. Specifically, the homogenization scheme en-
14 visaged cannot be realized without defining a common aerosol/cloud model that will
15 be applicable to all the missions. This includes also the definition of a common aero-
16 sol/cloud classification scheme for the space-borne products and ancillary ground-
17 based datasets and the derivation of aerosol/cloud-type-dependent AE for all lidar-
18 related properties, i.e., extinction, backscatter and depolarization. It is believed that
19 the well-established EARLINET network offers a unique opportunity to support such
20 an effort. Several EARLINET stations operate multi- wavelength Raman lidars, with
21 most of them measuring particle depolarization as well. Network's so-called "core
22 stations" deliver the entire CALIOP/ALADIN/ATLID parameter set, so that the BAEs
23 and EAEs for a variety of aerosol types can be derived experimentally over a compa-
24 rably long time period.

1 **ACKNOWLEDGMENTS**

2 This work has been developed under the auspices of the ESA-ESTEC project: Lidar
3 Climatology of Vertical Aerosol Structure for Space-Based LIDAR Simulation Stud-
4 ies (LIVAS) contract N°4000104106/11/NL/FF/fk. The publication was supported by
5 the European Union Seventh Framework Programme (FP7-REGPOT-2012-2013-1),
6 in the framework of the project BEYOND, under Grant Agreement No. 316210
7 (BEYOND - Building Capacity for a Centre of Excellence for EO-based monitoring
8 of Natural Disasters). The research leading to these results has received funding from
9 the European Union Seventh Framework Programme (FP7/2007-2013) under grant
10 agreement no 262254 (ACTRIS), grant agreement n° 606953 and grant agreement no
11 289923 – ITaRS. This research has been financed by EPAN II and PEP under the na-
12 tional action “Bilateral, multilateral and regional R&T cooperations” (AEROVIS Si-
13 no-Greek project). This work was performed in the framework of PROTEAS project
14 within GSRT’s KRIPIS action, funded by Greece and the European Regional Devel-
15 opment Fund of the European Union under the O.P. Competitiveness and Entrepre-
16 neurship, NSRF 2007-2013 and the Regional Operational Program of Attica.

17 The authors acknowledge EARLINET for providing aerosol lidar profiles available
18 under the World Data Center for Climate (WDCC) (“The EARLINET publishing
19 group 2000-2010, 2014 a, b, c, d, e). We thank the AERONET PIs and their staff for
20 establishing and maintaining the AERONET sites used in this investigation.
21 CALIPSO data were obtained from the ICARE Data Center (<http://www.icare.univ->
22 [lille1.fr/](http://www.icare.univ-lille1.fr/)). We would like to thank Jason Tackett for his support during the algorithm
23 development for the production of Level 3 CALIPSO products.

24

1 **TABLES**

2

3 **Table 1.** LIVAS aerosol model

aerosol type	LIVAS aerosol model									
	Size distribution parameters						Refractive index at 532 nm			
	fine mode			coarse mode			fine mode		coarse mode	
	median radius (µm)	standard deviation	total volume (µm ³ /µm ²)	median radius (µm)	standard deviation	total volume (µm ³ /µm ²)	real part	imag. part	real part	imag. part
polluted continental	0.2	0.5	0.08	2.8	0.68	0.05	1.45	0.006	1.45	0.006
smoke	0.17	0.5	0.05	3.7	0.65	0.03	1.47	0.018	1.47	0.018
dust	0.14	0.5	0.04	2.2	0.68	0.25	1.51	0.022	1.51	0.022
polluted dust	0.17	0.57	0.14	3.2	0.67	0.19	1.49	0.017	1.49	0.017
clean marine	0.16	0.5	0.22	2.6	0.72	1.5	1.41	0.002	1.36	0
clean continental	0.2	0.8	0.94	5.97	0.92	0.6	1.42	0.0023	1.53	0.008

4

5 **Table 2.** BAE and EAE for each aerosol type used in LIVAS for the conversion from 532 to
6 355 nm (VIS-UV) and from 532 to 1570 and 2050 nm (VIS-IR). The approaches used for
7 their calculation are also indicated.

LIVAS AEROSOL TYPE	UV/VIS			VIS/IR				
	approach used	532/355 nm		approach used	532/1570 nm		532/2050 nm	
		BAE	EAE		BAE	EAE	BAE	EAE
Polluted continental	ESA-CALIPSO	1.42	1.24	AERONET-Omar	1.18	1.66	1.32	1.56
Dust	ESA-CALIPSO	0.40	0.55	AERONET-CALIPSO	0.35	0.6	0.43	0.57
Polluted dust	ESA-CALIPSO	0.92	0.71	AERONET-CALIPSO	0.67	1.14	0.71	1.07
Smoke	ESA-CALIPSO	1.46	1.41	AERONET-CALIPSO	0.79	1.42	0.825	1.34
Clean marine	ESA-CALIPSO (bsc) Sayer et al. (2012) (ext)	0.50	0.78	Sayer et al. (2012)	0.74	0.39	0.81	0.38
Clean continental	ESA-CALIPSO (bsc) OPAC (ext)	1.20	1.31	OPAC	1.15	1.28	1.64	1.27
Stratospheric	ESA-CALIPSO (bsc) Deshler et al. (1993), Wandinger et al. (1995) (ext)	0.98	0.48	Deshler et al. (1993), Wandinger et al. (1995)	1.36	1.33	1.38	1.49

1

2 **Table 3.** LIVAS and CALIPSO LR, SSA and effective radius.

3

aerosol type	LIVAS aerosol model			CALIPSO aerosol model		
	LR at 532 nm (sr)	SSA at 532 nm	effective radius (μm)	LR at 532 nm (sr)	SSA at 532 nm	effective radius (μm)
polluted continental	64	0.95	0.28	70	0.93	0.26
smoke	90	0.88	0.26	70	0.8	0.36
dust	85	0.87	0.65	40	0.9	0.43
polluted dust	82	0.89	0.35	65	0.8	0.43
clean marine	31	0.98	0.75	20	0.99	0.93
clean continental	54	0.96	0.26	35	0.88	1.4

4

5

1 **FIGURE CAPTIONS**

2 **Figure 1.** The data and methods used for the derivation of LIVAS BAEs and EAEs in
3 the UV and IR.

4

5 **Figure 2:** BAEs (upper) and EAEs (bottom) calculated with different approaches (i.e.
6 “AERONET-Omar” (red triangles), “AERONET-CALIPSO” (green triangles), “Sayer
7 et al. (2012)” (cyan triangles), “OPAC” (pink triangles)) and validated against the
8 ESA-CALIPSO BAEs and EAE in VIS and UV (black circles). The BAEs and EAEs
9 selected and ingested in the LIVAS aerosol model for the VIS-IR conversions, are
10 denoted with symbols of larger size.

11

12 **Figure 3:** Comparison of the mean volume size distributions for each aerosol type in
13 the LIVAS (blue line) and CALIPSO (pink line) aerosol models.

14

15 **Figure 4:** Comparison of the mean real part of the refractive index for each aerosol
16 type in the LIVAS (blue line) and CALIPSO (pink line) aerosol models.

17

18 **Figure 5:** Comparison of the mean imaginary part of the refractive index for each
19 aerosol type in the LIVAS (blue line) and CALIPSO (pink line) aerosol models.

20

21 **Figure 6:** Comparison of the mean spectral SSA for each aerosol type in the LIVAS
22 (blue line) and CALIPSO (pink line) aerosol models.

23

24 **Figure 7:** Comparison of LIVAS and CALIPSO with ESA-CALIPSO values for:
25 BAE at 355/532 nm (upper-left), EAE at 355/532 nm (upper-right), lidar ratio at 532
26 nm (lower-left) and effective radius (lower-right).

27

28 **Figure 8:** CALIPSO Level 2 extinction coefficient profile at 532 nm (left), aerosol
29 type (center) and converted extinction coefficient at 355 nm (right), based on LIVAS
30 typical EAEs. The profile example refers to September 7th, 2011, (cell centroid with
31 latitude of 37.5 and longitude of 20.5 degrees).

32

33 **Figure 9.** Schematic diagram of LIVAS processing chain.

34

35 **Figure 10.** LIVAS aerosol extinction products. Upper panel: vertical distribution of
36 the averaged aerosol extinction coefficient at 355, 532, 1064, 1570, 2050 nm (left),
37 number of observations used in averaging (right). Middle panel: vertical distribution
38 of the averaged aerosol extinction coefficient per aerosol type (left), number of obser-
39 vations used in averaging (right). Lower panel: vertical distribution of the averaged
40 aerosol extinction coefficient per season (left), number of observations used in aver-
41 aging (right).

42

43 **Figure 11.** Additional LIVAS products: Upper panel: vertical distribution of the aver-
44 aged particle depolarization at 532 nm (left), number of observations used in averag-
45 ing (right). Middle panel: vertical distribution of the averaged cloud extinction coeffi-
46 cient per season (left), number of observations used in averaging (right). Lower panel:
47 vertical distribution of the averaged stratospheric aerosol extinction coefficient (left),
48 number of observations used in averaging (right).

49

1 **Figure 12.** Spatial distribution of the 532 nm AOD absolute differences (absolute val-
2 ue of LIVAS averaged AOD minus AERONET averaged AOD) (blue circles) and of
3 the difference between AERONET site elevation and mean grid cell elevation of
4 CALIPSO overpass (red crosses).

5
6 **Figure 13.** Example of high-slope terrain on CALIPSO overpass for the case of
7 ND_Marbel_Univ AERONET station. Left panel: vertical distribution of the averaged
8 aerosol extinction coefficient. Right panel: number of observations used in averaging.

9
10 **Figure 14.** Percentiles of the number of overpasses in LIVAS global grid cells.

11
12 **Figure 15.** Spatial distribution of the 532 nm AOD absolute biases (LIVAS averaged
13 AOD minus AERONET averaged AOD).

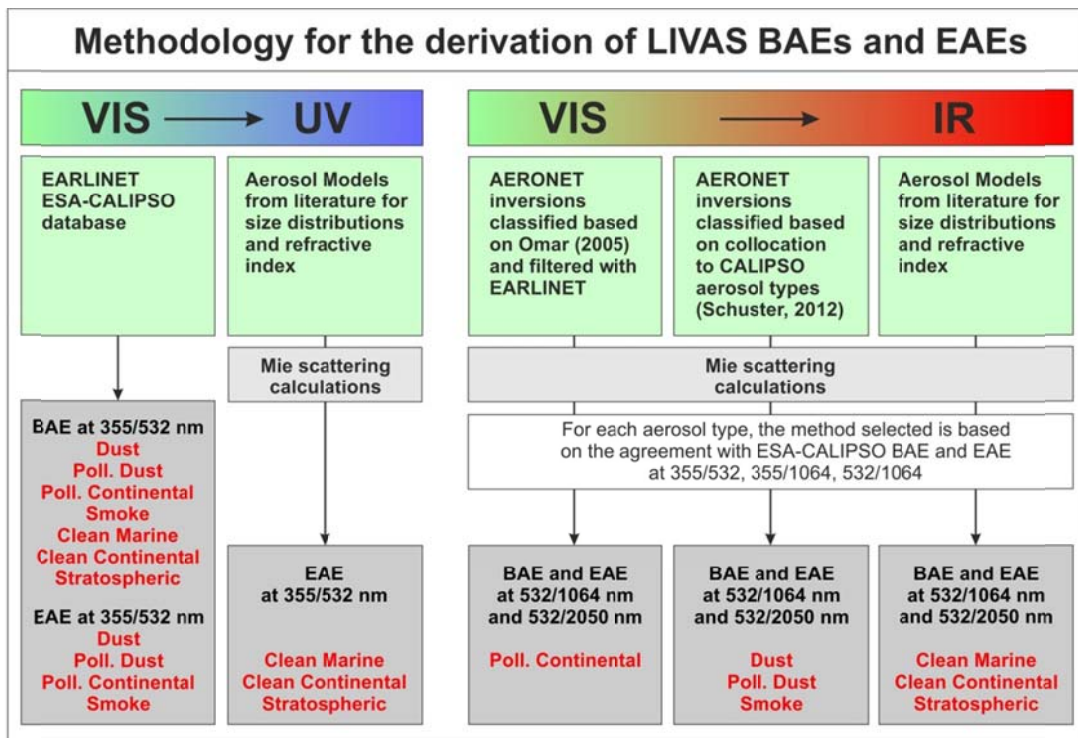
14
15 **Figure 16.** Upper panel: Scatter plot comparison of LIVAS AODs at 532 nm versus
16 collocated AERONET Level 2 product (left) and standard deviation of the LIVAS
17 AODs versus standard deviation of the AERONET AODs at 532 nm (right). Lower
18 panel: Scatter plot comparison of LIVAS AODs at 355 nm versus collocated
19 AERONET Level 2 product (left) and of LIVAS AODs at 1570 nm versus collocated
20 AERONET Level 2 product (right).

21
22 **Figure 17.** The LIVAS web-portal.

23
24 **Figure 18.** Global distribution of LIVAS AOD at 532 nm.

25

2 FIGURES

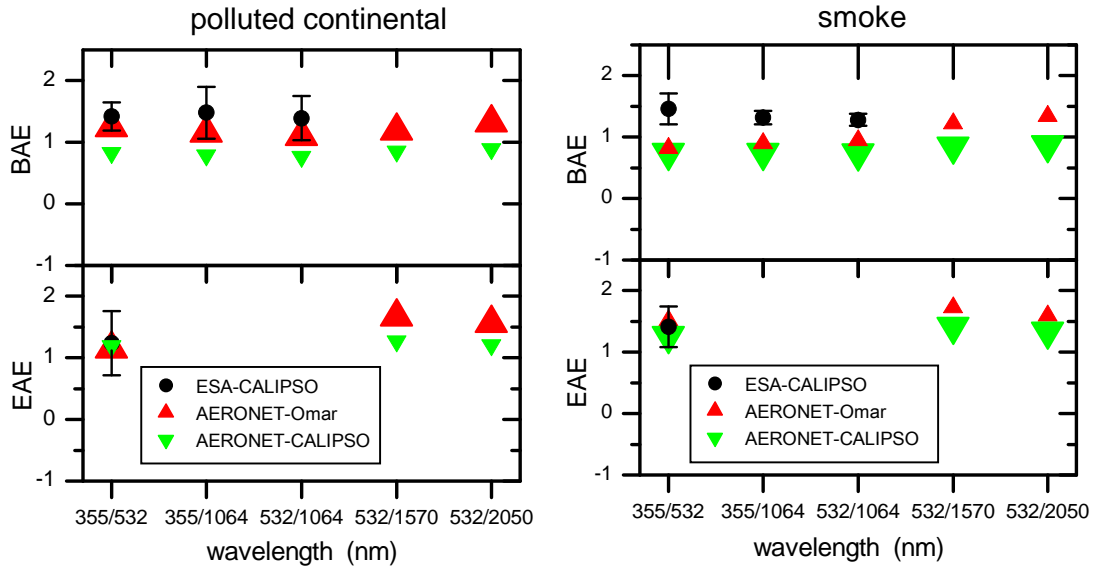


3

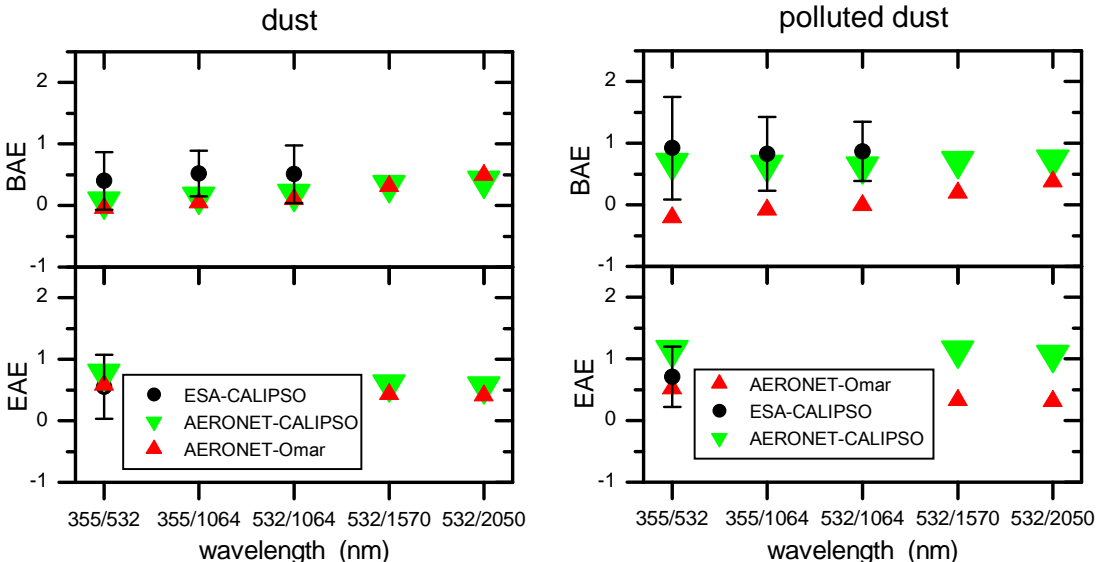
4

5

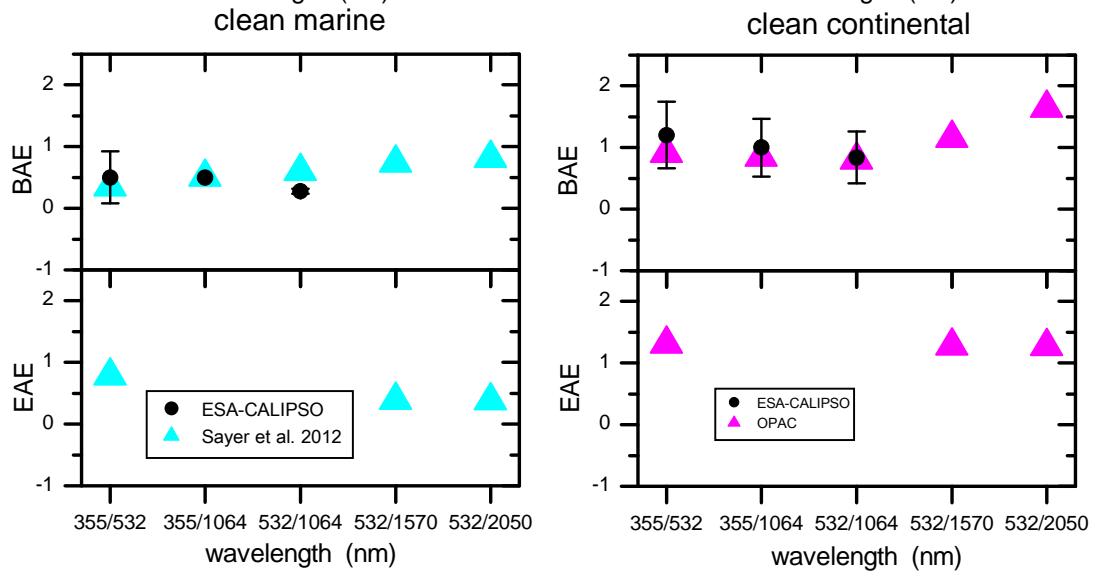
Figure 1



1



2



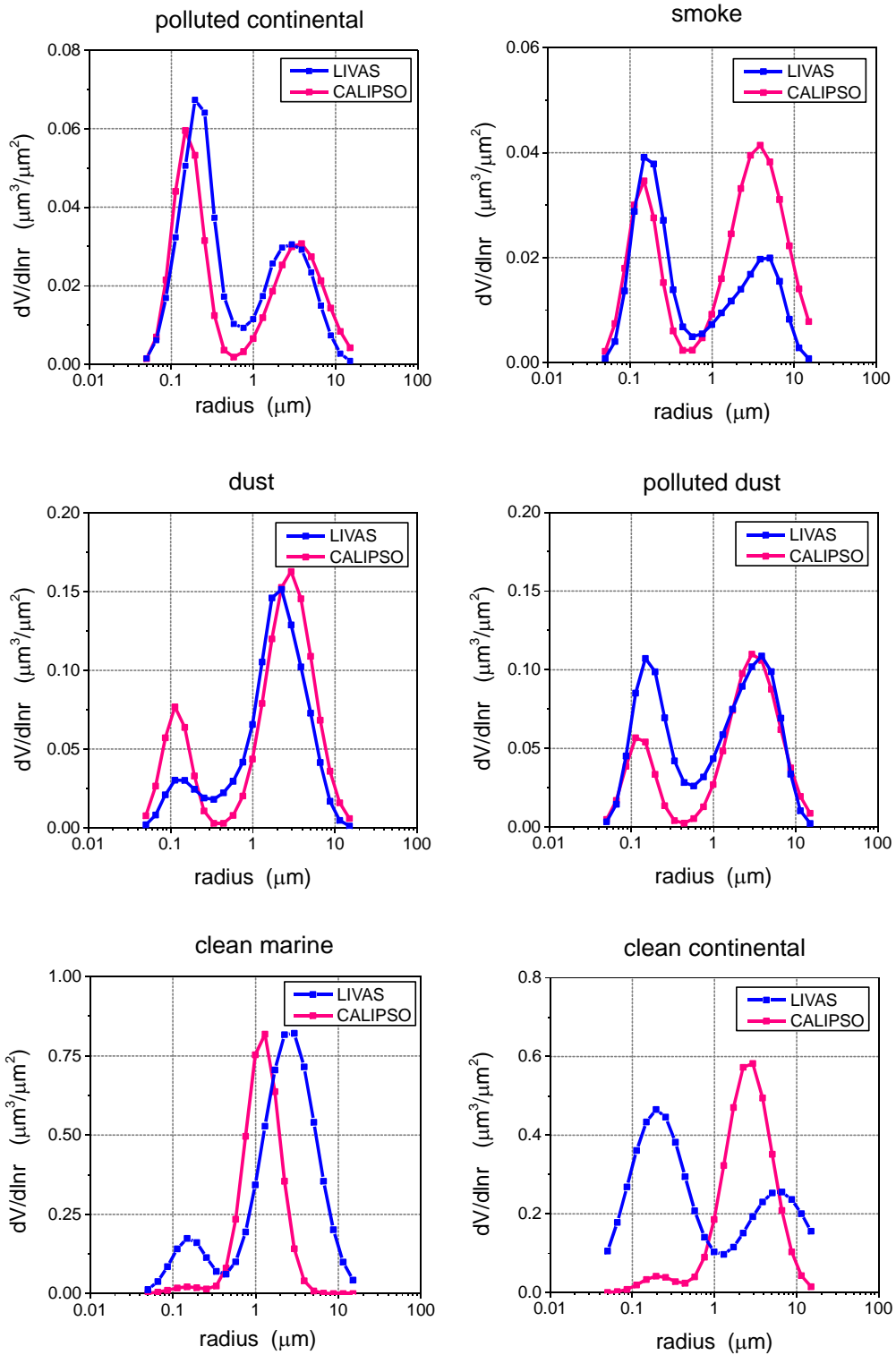
3

4

5

Figure 2

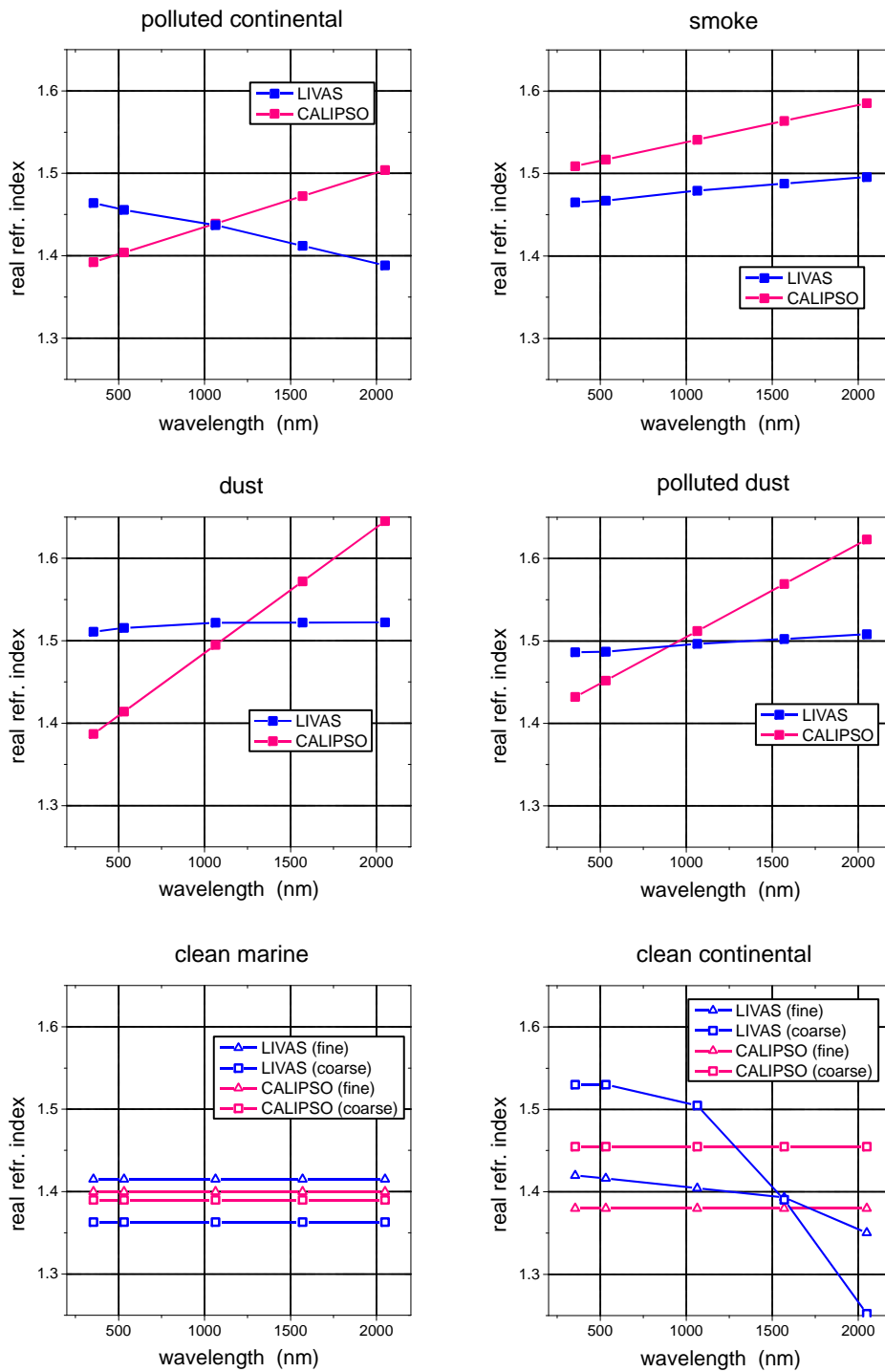
1



2
3
4
5

Figure 3

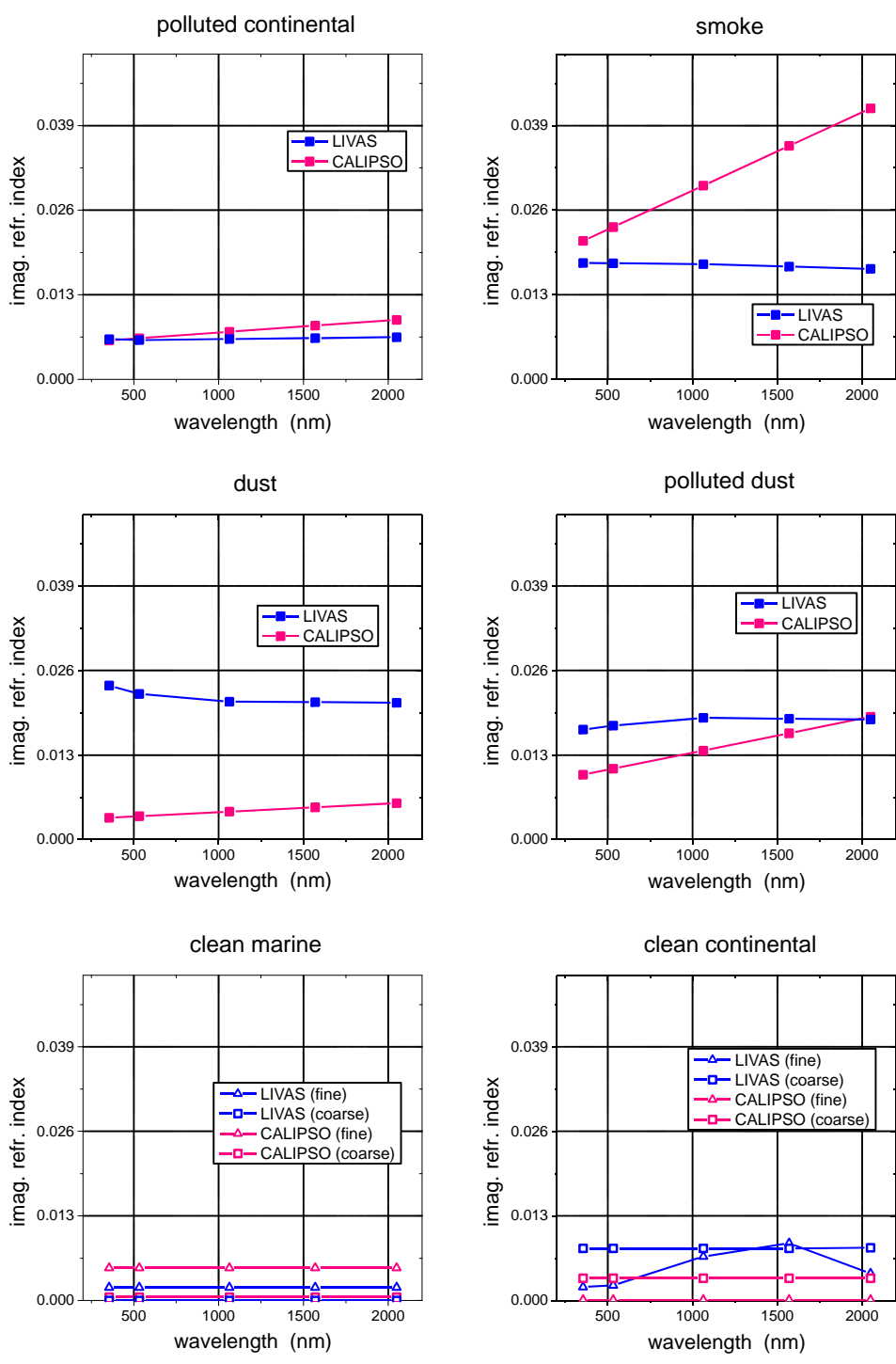
1
2



3
4
5
6

Figure 4

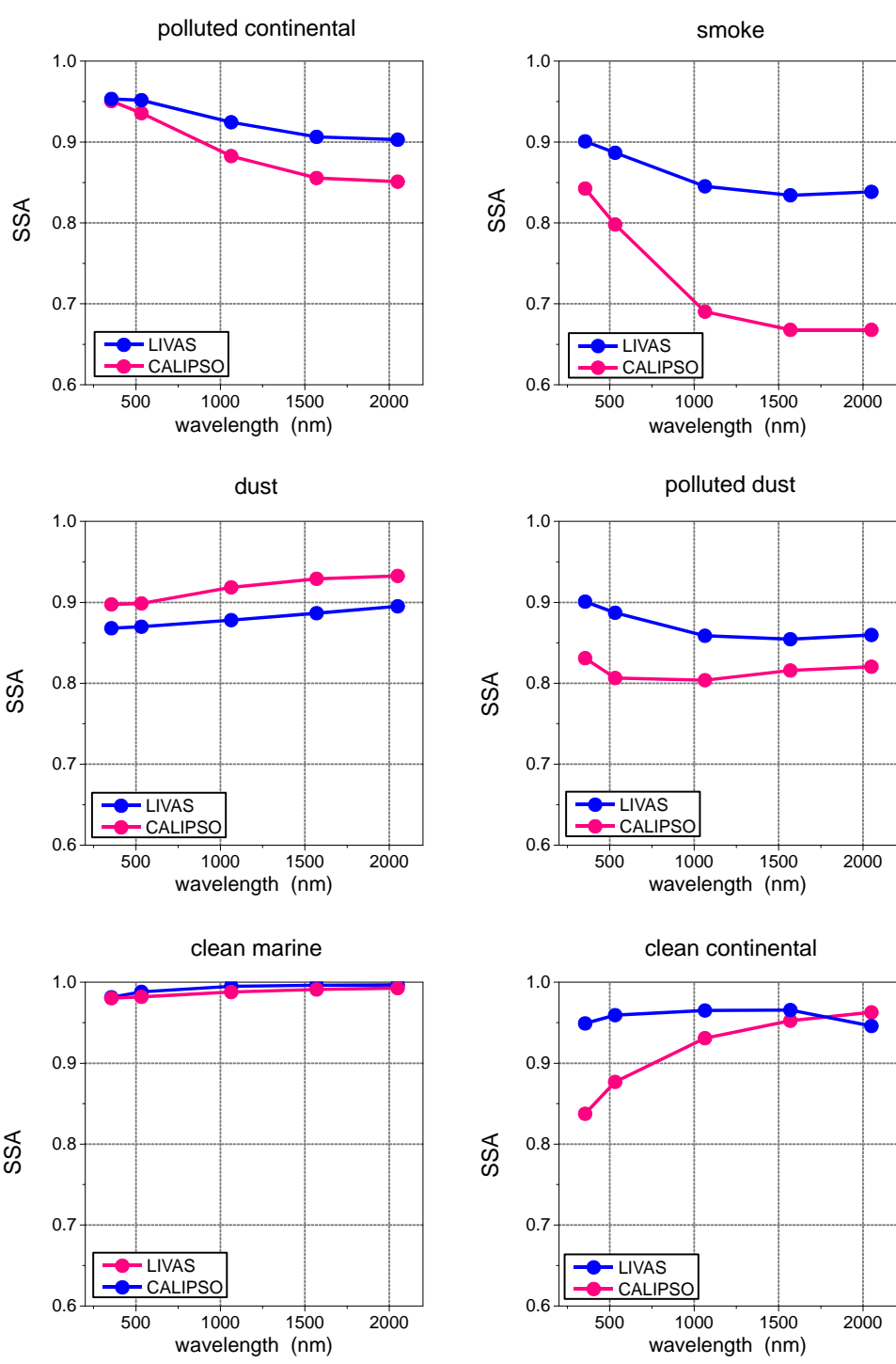
1
2



3
4
5
6

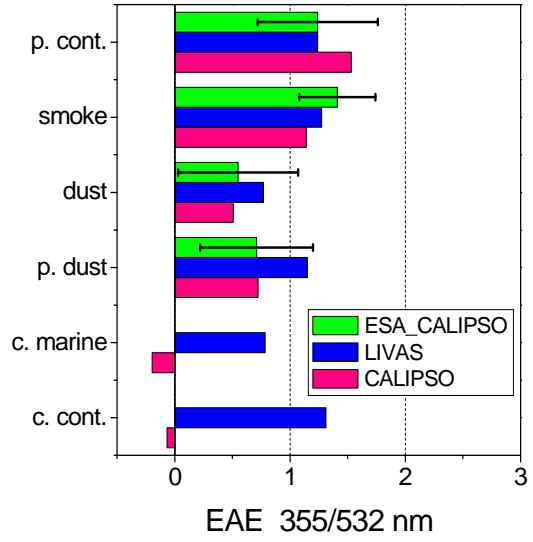
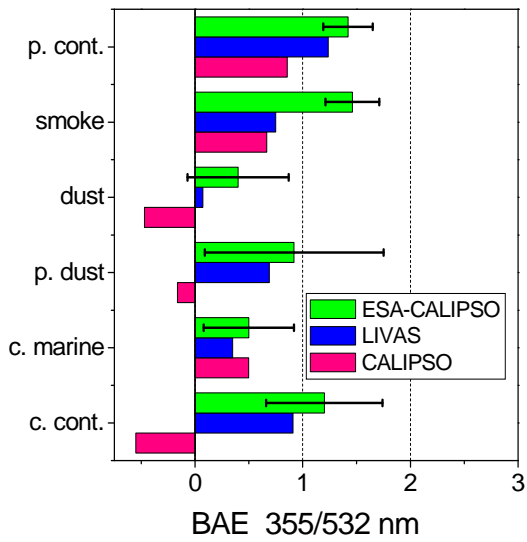
Figure 5

1
2
3

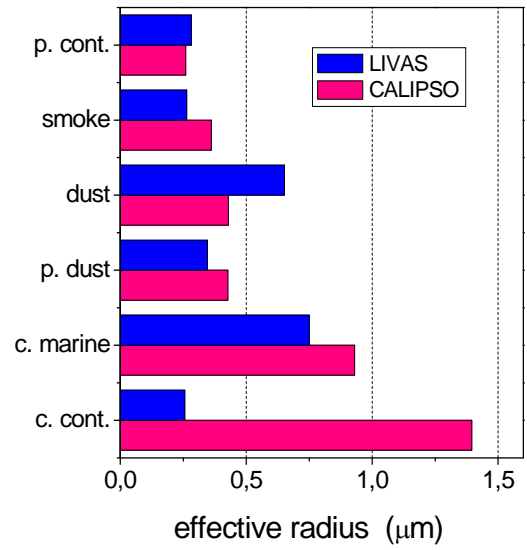
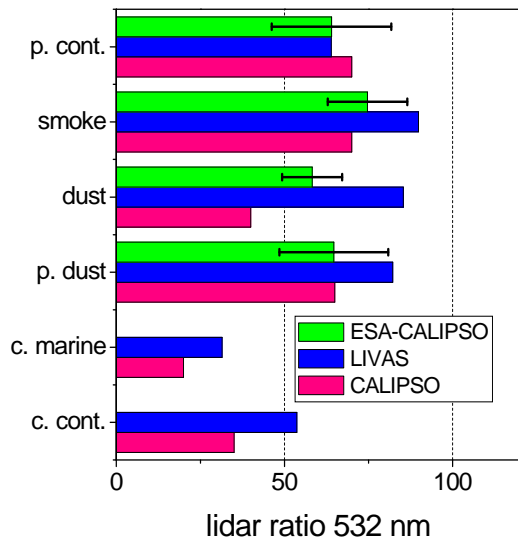


4
5
6
7
8
9
10

Figure 6

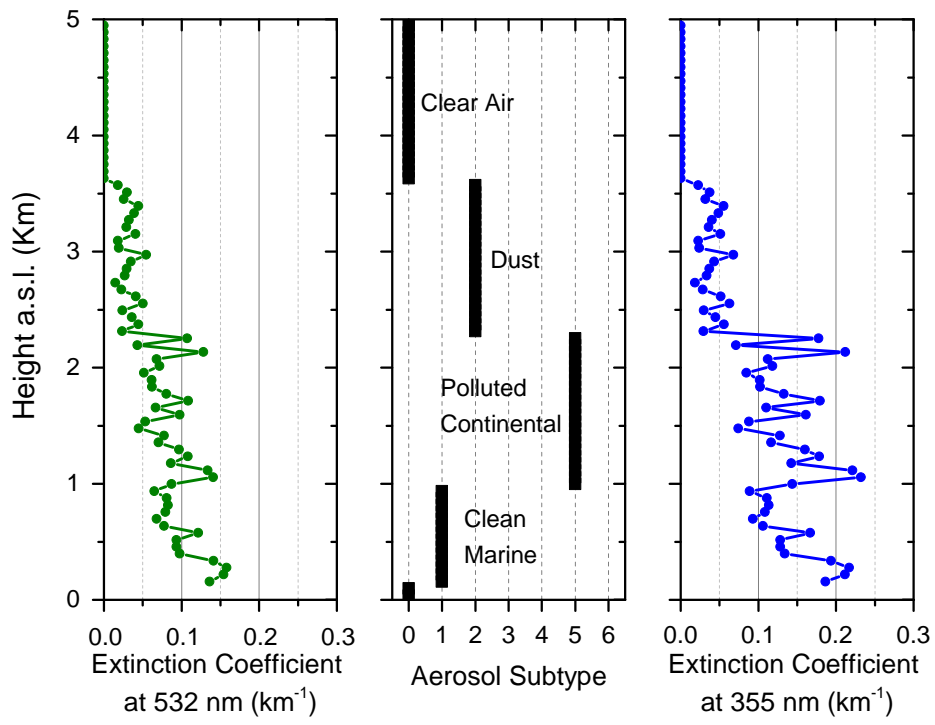


1
2



3
4
5
6
7
8

Figure 7



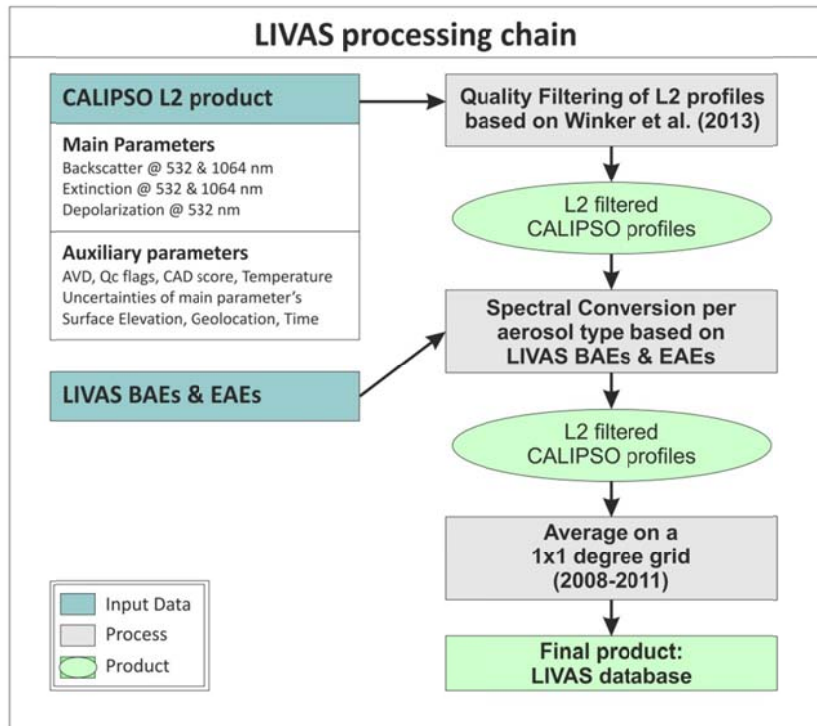
1

2

3

Figure 8

2



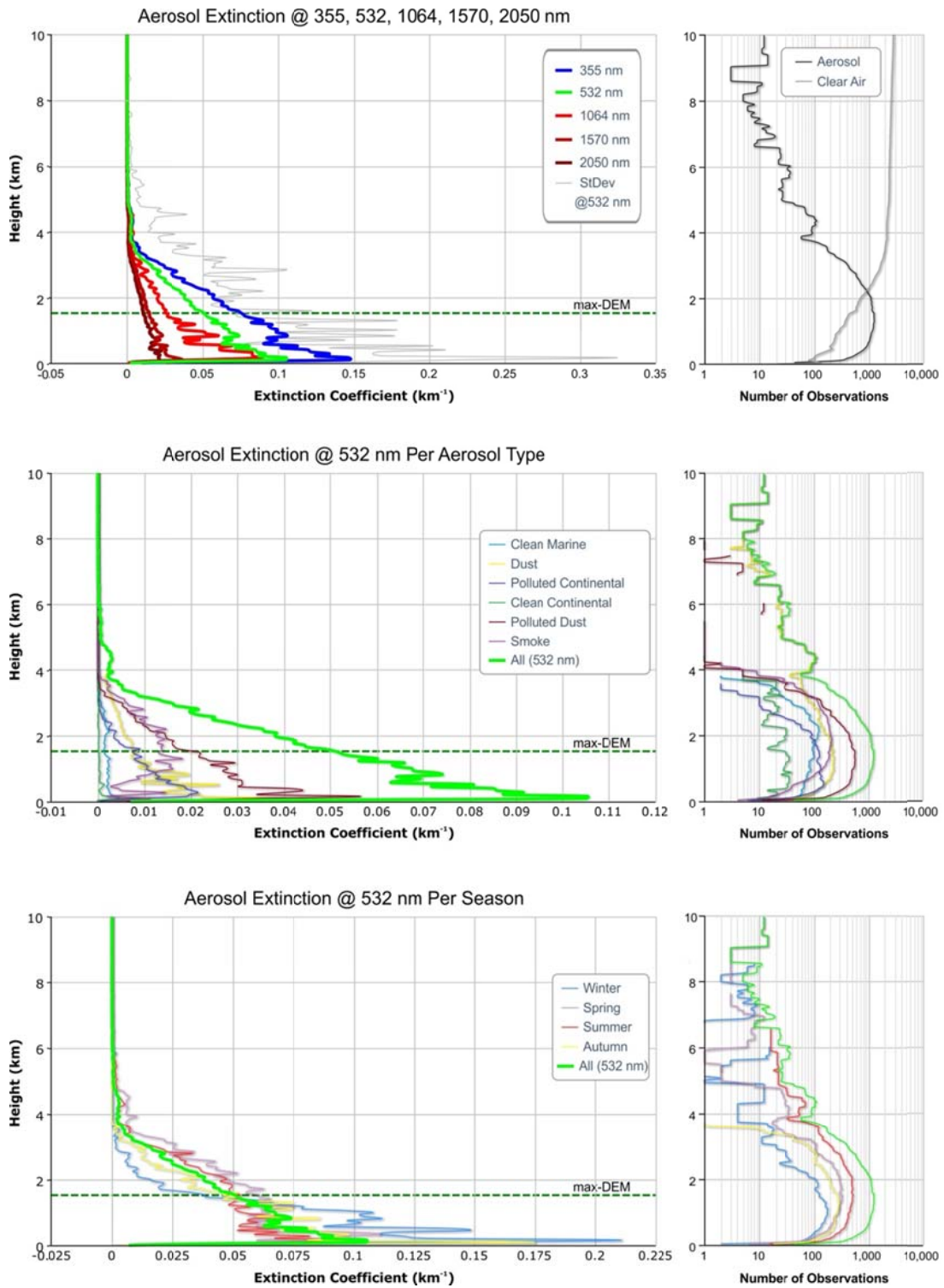
3

4

5

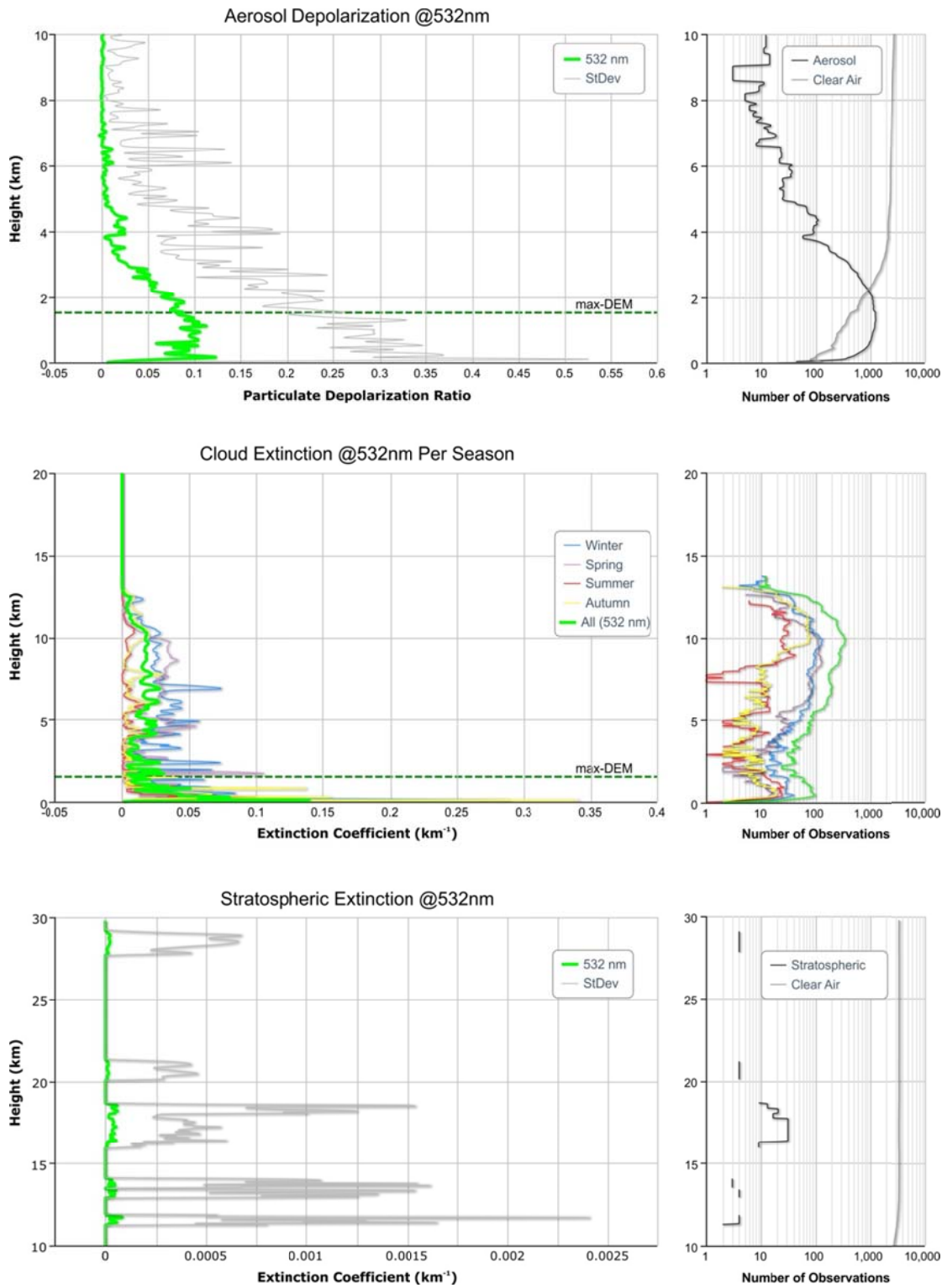
6

Figure 9



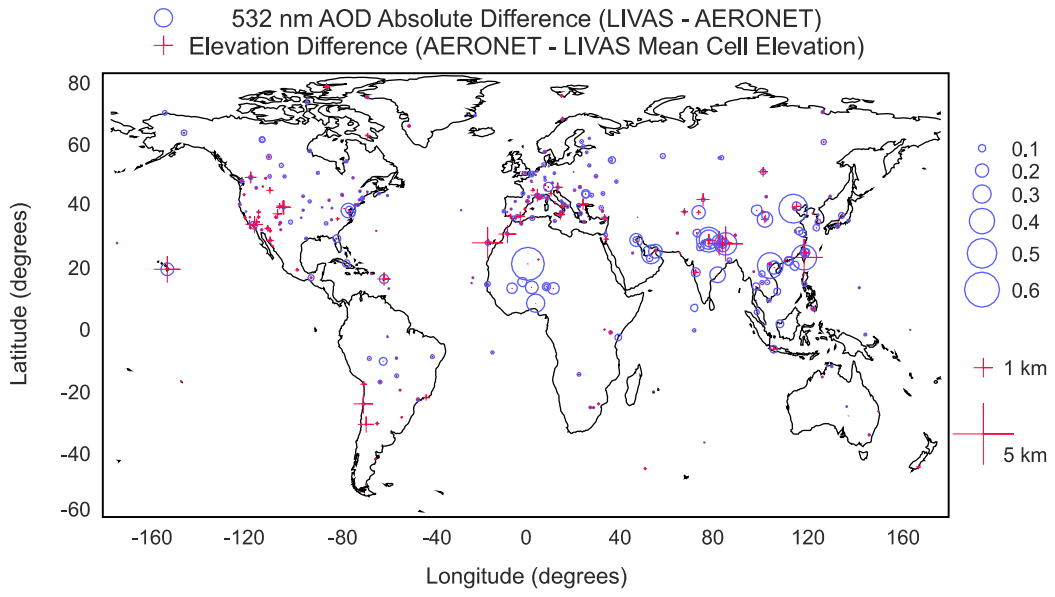
2
3
4

Figure 10



2
3
4

Figure 11

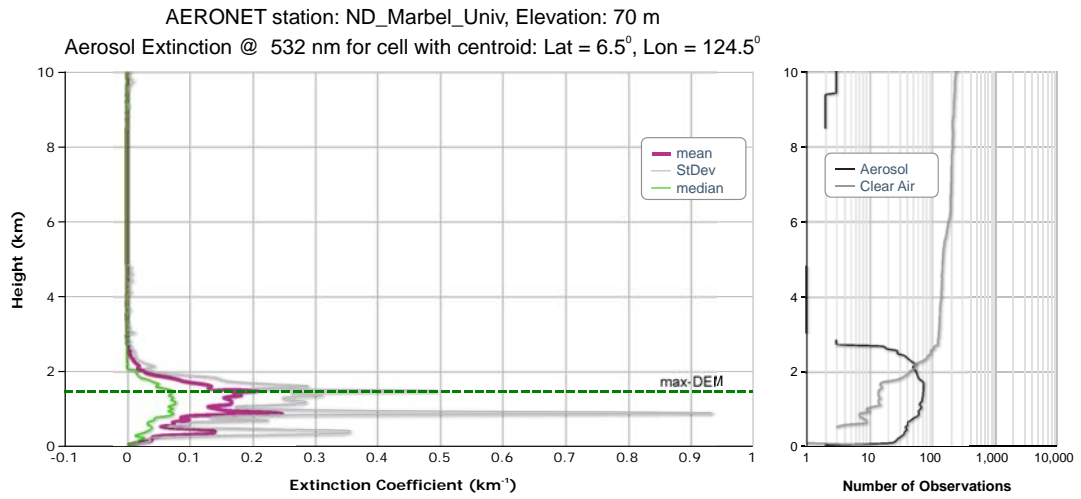


1

2

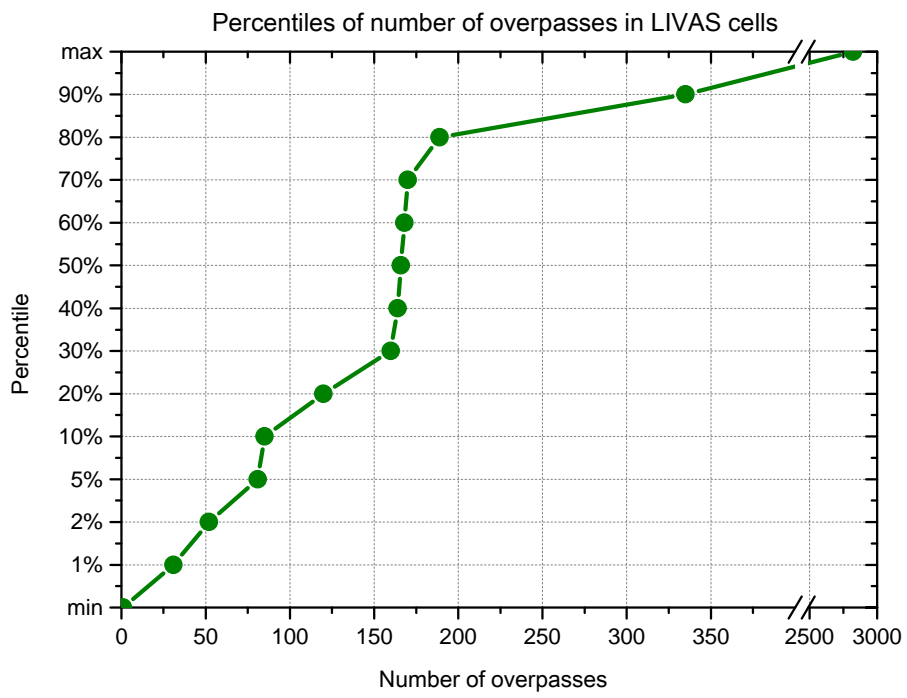
3

Figure 12



- 1
- 2
- 3
- 4

Figure 13



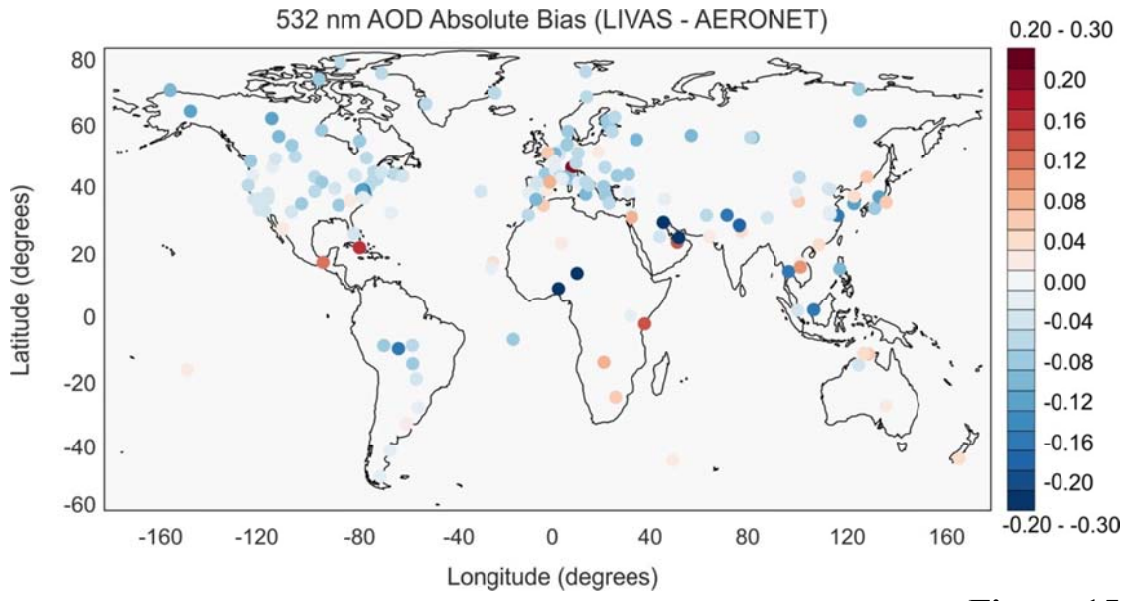
1

2

3

Figure 14

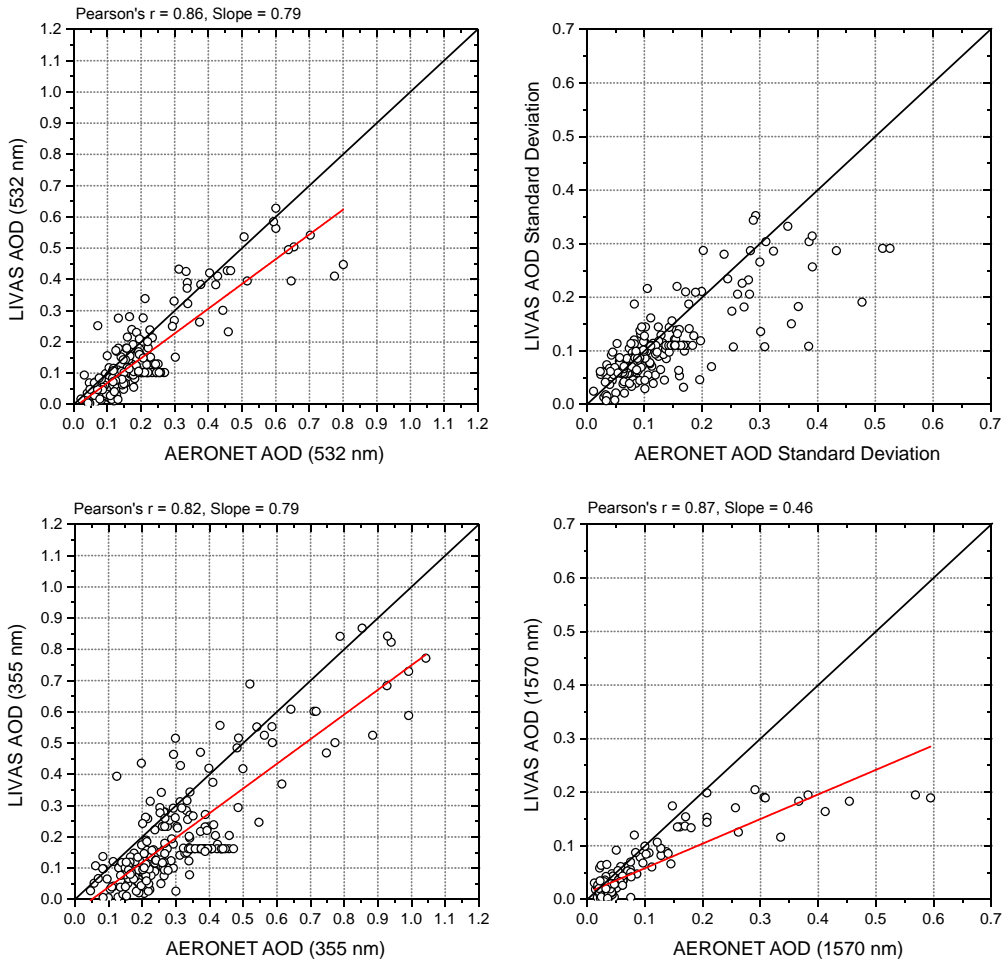
2



3
4
5
6
7

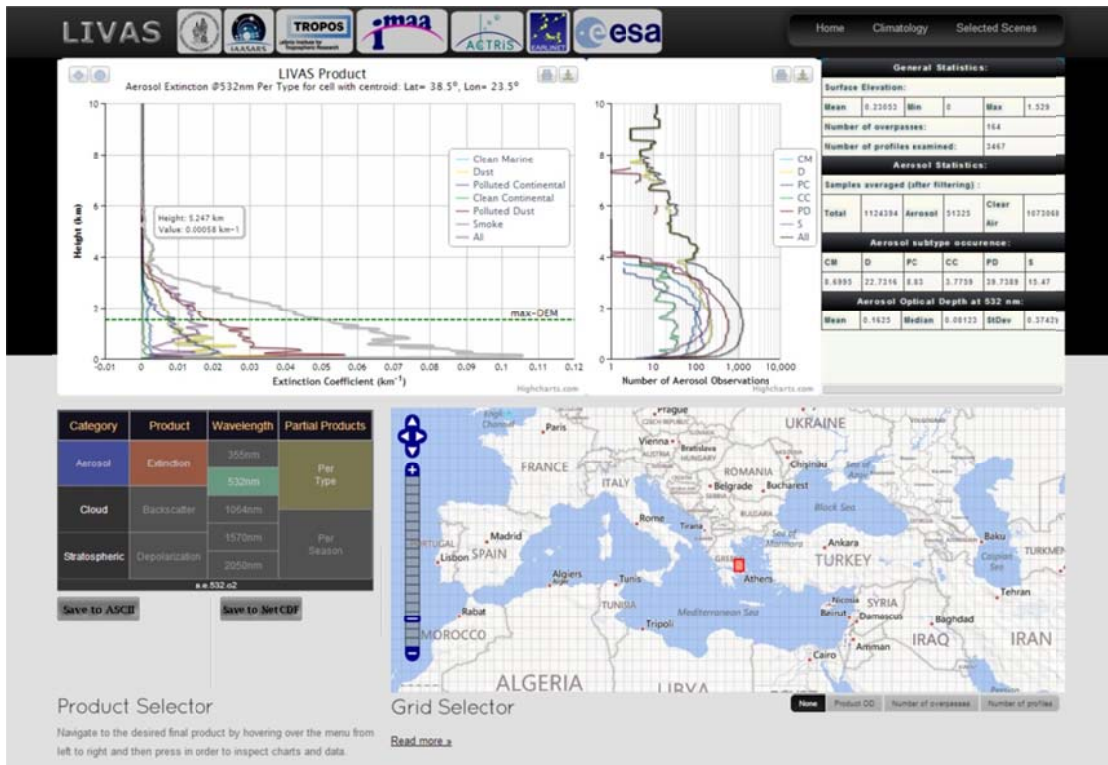
Figure 15

1
2
3



4
5
6

Figure 16

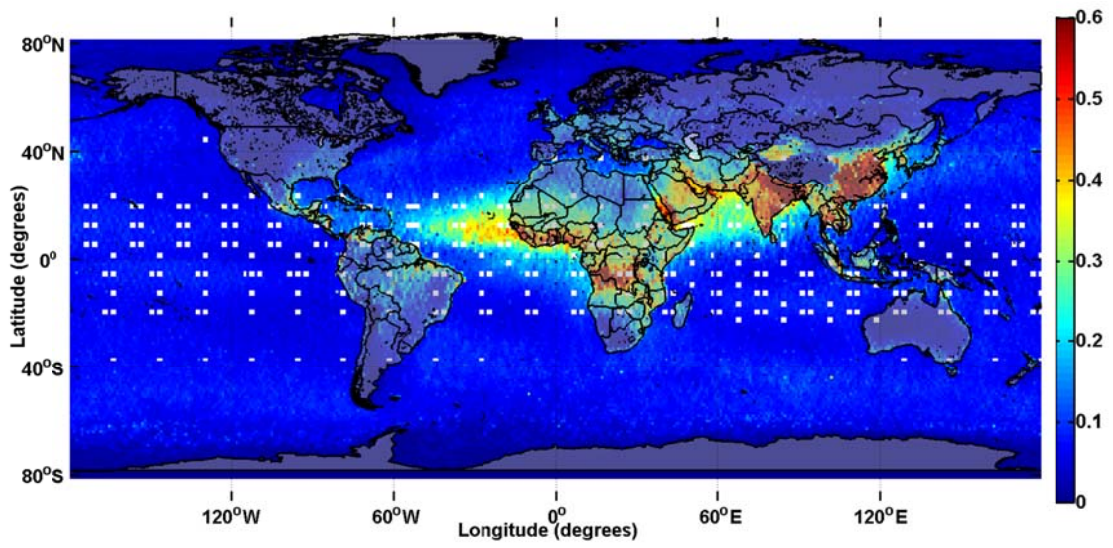


2

3

4

Figure 17



2

3

4

5

6

7

8

9

Figure 18

1 REFERENCES

- 2 Amiridis, V., Wandinger, U., Marinou, E., Giannakaki, E., Tsekeri, A., Basart, S.,
3 Kazadzis, S., Gkikas, A., Taylor, M., Baldasano, J., and Ansmann, A., Optimizing
4 CALIPSO Saharan dust retrievals, *Atmos. Chem. Phys.*, 13, 12089-12106,
5 doi:10.5194/acp-13-12089-2013, 2013.
- 6 Böckmann C., et al., Aerosol lidar intercomparison in the framework of the
7 EARLINET project. 2. Aerosol backscatter algorithms, *Appl. Opt.* 43, 977-989, 2004.
- 8 Bösenberg, J., Matthias, V., Amodeo, A., Amiridis, V., Ansmann, A., et al.,
9 EARLINET: A European Aerosol Research Lidar Network to Establish an Aerosol
10 Climatology, Max-Planck-Institut Report No. 348, 2003.
- 11 Burton, S. P., Ferrare, R. A., Vaughan, M. A., Omar, A. H., Rogers, R. R.,
12 Hostetler, C. A., and Hair, J. W., Aerosol classification from airborne HSRL and
13 comparisons with the CALIPSO vertical feature mask, *Atmos. Meas. Tech.*, 6, 1397-
14 1412, doi:10.5194/amt-6-1397-2013, 2013.
- 15 Campbell, J. R., Reid, J. S., Westphal, D. L., Zhang, J., Tackett, J. L., Chew, B. N.,
16 Welton, E. J., Shimizu, A., Sugimoto, N., Aoki, K., and Winker, D. M., Characteriz-
17 ing the vertical profile of aerosol particle extinction and linear depolarization over
18 Southeast Asia and the Maritime Continent: the 2007–2009 view from CALIOP, *At-
19 mos. Res.*, doi:10.1016/j.atmosres.2012.05.007, 2012.
- 20 Deshler, T., Johnson, B. J., & Rozier, W. R., Balloonborne measurements of Pinatubo
21 aerosol during 1991 and 1992 at 41° N: vertical profiles, size distribution, and vola-
22 tility. *Geophys. Res. Lett.* 20, 1435–1438, 1993.
- 23 Dubovik, O., and King, M. D., A flexible inversion algorithm for retrieval of aerosol
24 optical properties from sun and sky radiance measurements, *J. Geophys. Res.*, 105,
25 20,673–20,696, 2000.
- 26 Dubovik, O., Smirnov, A., Holben, B. N., King, M. D., et al., Accuracy assessments
27 of aerosol optical properties retrieved from Aerosol Robotic Network (AERONET)
28 Sun and sky radiance measurements, *J. Geophys. Res.*, 105, 9791– 9806, 2000.

1 Dubovik, O., Sinyuk, A., Lapyonok, T., Holben, B. N., Mishchenko, M., Yang, P.,
2 Eck, T. F., Volten, H., Muñoz, O., Veihelmann, B., van der Zande, W. J., Leon, J.-F.,
3 Sorokin, M. and Slutsker, I.: Application of spheroid models to account for aerosol
4 particle nonsphericity in remote sensing of desert dust, *J. Geophys. Res.*, 111(D11),
5 D11208, doi:10.1029/2005JD006619, 2006.ESA, Reports for Mission Selection, The
6 Six Candidate Earth Explorer Missions, EarthCARE – Earth Clouds, Aerosols and
7 Radiation Explorer, ESA-SP-1279(1), 2004.

8 Eck, T. F., Holben, B. N., Slutsker, I. and Setzer, A.: Measurements of irradiance at-
9 tenuation and estimation of aerosol single scattering albedo for biomass burning aero-
10 sols in Amazonia, *J. Geophys. Res.* 103, 31865-31878, 1998.

11 Eck, T. F., Holben, B. N., Reid, J. S., Dubovik, O., Smirnov, A., O’Neill, N. T.,
12 Slutsker, I., and Kinne, S.: Wavelength dependence of the optical depth of biomass
13 burning, urban, and desert dust aerosols, *J. Geophys. Res.*, 104(D24), 31,333–31,349,
14 1999.

15 Eck, T. F., Holben, B. N., Reid, J. S., O’Neill, N. T., Schafer, J. S., Dubovik, O.,
16 Smirnov, A., Yamasoe, M. A. and Artaxo, P.: High aerosol optical depth biomass
17 burning events: A comparison of optical properties for different source regions, *Ge-*
18 *ophys. Res. Lett.*, 30, 2035, doi:10.1029/2003GL017861, 20, 2003.

19 Freudenthaler, V., et al., Depolarization ratio profiling at several wavelengths in pure
20 Saharan dust during SAMUM 2006, *Tellus, Ser. B*, 61, 165–179, doi:10.1111/j.1600–
21 0889.2008.00396.x., 2009.

22 Freudenthaler, V., et al., EARLI09 – direct intercomparison of eleven EARLINET
23 lidar systems, in: *Proceedings of the 25th International Laser Radar Conference*, St.
24 Petersburg, Russia, 5–9 July, 891–894, 2010.

25 Groß, S., Tesche, M., Freudenthaler, V., Toledano, C., Wiegner, M., Ansmann, A.,
26 Althausen, D. & Seefeldner, M., Characterization of Saharan dust, marine aerosols
27 and a mixture of biomass burning aerosols and dust by means of multiwavelength de-
28 polarization and Raman measurements during SAMUM-2, *Tellus, Ser. B*, 63, 706–
29 724. doi: 10.1111/j.1600-0889.2011.00556.x, 2011a.

1 Groß, S., et al., Dual-wavelength linear depolarization ratio of volcanic aerosols: Li-
2 dar measurements of the Eyjafjallajökull plume over Maisach, Germany, *Atm. Envi-
3 ron.*, doi:10.1016/j.atmosenv.2011.06.017, 2011b.

4 Hasekamp, O., Litvinov, P., and Butz, A.: Aerosol properties over the ocean from
5 PARASOL multi-angle photopolarimetric measurements, *J. Geophys. Res.*, 116,
6 D14204, doi:10.1029/2010JD015469, 2011.

7 Hess, M., Köpke, P. & Schult, I., Optical properties of aerosols and clouds: the soft-
8 ware package OPAC. *Bull. Am. Meteorol. Soc.* 79, 831–844, 1998.

9 Holben, B. N., Eck, T. F., Slutsker, I., Tanre, D., Buis, J. P., Setzer, A., Vermote, E.,
10 Reagan, J. A., Kaufman, Y. J. and Nakajima, T.: AERONET—A federated instrument
11 network and data archive for aerosol characterization, *Remote sensing of environ-
12 ment*, 66(1), 1–16, 1998.

13 Holben, B. N., Tanré, D., Smirnov, A., Eck, T. F., Slutsker, I., Abuhassan, N., New-
14 comb, W. W., Schafer, J. S., Chatenet, B., Lavenu, F., Kaufman, Y. J., Vande Castle,
15 J., Setzer, A., Markham, B., Clark, D., Frouin, R., Halthore, R., Karneli, A., O'Neill,
16 N. T., Pietras, C., Pinker, R. T., Voss, K., and Zibordi, G.: An emerging ground-based
17 aerosol climatology: Aerosol optical depth from AERONET, *J. Geophys. Res. D: At-
18 mospheres*, 106(D11), 12067-12097, doi:10.1029/2001JD900014, 2001.

19 Holler, R., Ito, K., Tohno, S., and Kasahara, M.: Wavelengthdependent aerosol single-
20 scattering albedo: Measurements and model calculations for a coastal site near the Sea
21 of Japan during ACE-Asia, *J. Geophys. Res.*, 108(D23), 8648,
22 doi:10.1029/2002JD003250, 2003.

23 Illingworth, A., Barker, H., Beljaars, A., Ceccaldi, M., Chepfer, H., Colec, J., Dela-
24 noe, J., Domenech, C., Donovan, D., Fukuda, S., Hirakata, M., Hogan, R.,
25 Huenerbein, A., Kollias, P., Kubota, T., Nakajima, T., Nakajima, T., Nishizawa, T.,
26 Ohno, Y., Okamoto, H., Oki, R., Sato, K., Satoh, M., Shephard, M., Wandinger, U.,
27 Wehr, T., Zadelhoff, G-J., The EARTHCARE satellite: the next step forward in glob-
28 al measurements of clouds, aerosols, precipitation and radiation, BAMS-D-12-00227,
29 2014 (in print).

1 Jung, J., Kim, Y. J., Lee, K. Y., -Cayetano, M. G., Batmunkh, T., Koo, J.-H., and
2 Kim, J.: Spectral optical properties of long-range transport Asian dust and pollution
3 aerosols over Northeast Asia in 2007 and 2008, *Atmos. Chem. Phys.*, 10, 5391-5408,
4 doi:10.5194/acp-10-5391-2010, 2010.

5 Kanitz, T., Ansmann, A., Foth, A., Seifert, P., Wandinger, U., Engelmann, R.,
6 Baars, H., Althausen, D., Casiccia, C., and Zamorano, F., Surface matters: limitations
7 of CALIPSO V3 aerosol typing in coastal regions, *Atmos. Meas. Tech. Discuss.*, 7,
8 1333-1365, doi:10.5194/amtd-7-1333-2014, 2014.

9 Kim, S.-W., Yoon, S.-C., Kim, J., and Kim, S.-Y.: Seasonal and monthly variations of
10 columnar aerosol optical properties over East Asia determined from multi-year
11 MODIS, LIDAR, and AERONET Sun/sky radiometer measurements, *Atmos. Envi-
12 ron.*, 41, 1634–1651, 2007.

13 Koepke, P., Gasteiger, J., and Hess, M.: Technical Note: Optical properties of desert
14 aerosol with non-spherical mineral particles: data incorporated to OPAC, *Atmos.
15 Chem. Phys.*, 15, 5947-5956, doi:10.5194/acp-15-5947-2015, 2015.

16 Liu, Z., Vaughan, M., Winker, D., Kittaka, C., Getzewich, B., Kuehn, R., Omar, A.,
17 Powell, K., Trepte, C., and Hostetler, C.: The CALIPSO Lidar Cloud and Aerosol
18 Discrimination: Version 2 Algorithm and Initial Assessment of Performance. *J. At-
19 mos. Oceanic Technol.*, 26, 1198–1213, doi:10.1175/2009jtecha1229.1, 2009.

20 Mamouri, R. E., Ansmann, A., Nisantzi, A., Kokkalis, P., Schwarz, A., and
21 Hadjimitsis, D.: Low Arabian dust extinction-to-backscatter ratio, *Geophys. Res.
22 Lett.*, 40, doi:10.1002/grl.50898, 2013.

23 Matthias V., et al., Aerosol lidar inter-comparison in the framework of the
24 EARLINET project. 1 Instruments, *Appl. Opt.*, 43, N. 4, 961-976, 2004.

25 McConnell, C. L., Highwood, E. J., Coe, H., Formenti, P., Anderson, B., Osborne, S.,
26 Nava, S., Desboeufs, K., Chen, G., and Harrison, M. A. J.: Seasonal variations of the
27 physical and optical characteristics of Saharan dust: Results from the Dust Outflow
28 and Deposition to the Ocean (DODO) experiment, *J. Geophys. Res.*, 113, D14S05,
29 doi:10.1029/2007JD009606, 2008.

- 1 Mie, G., Beiträge zur Optik trüber Medien, speziell kolloidaler Metallösungen, *Ann.*
2 *Phys.*, 25(4), 377–445, 1908.
- 3 Mishchenko, M. I., Travis, L. D., and Lacis, A. A., *Scattering, Absorption, and Emis-*
4 *sion of Light by Small Particles*, Cambridge Univ. Press, New York, 2002. (Available
5 at <http://www.giss.nasa.gov/~crmim/books.html>)
- 6 Mueller, D., A. Ansmann, I. Mattis, M. Tesche, U. Wandinger, D. Althausen, and G.
7 Pisani, Aerosol-type-dependent lidar ratios observed with Raman lidar, *J. Geophys.*
8 *Res.*, 112, D16202, doi:10.1029/2006JD008292, 2007.
- 9 Müller, T., Schladitz, A., Massling, A., Kaaden, N., Wiedensohler, A., Kandler, K.:
10 Spectral absorption coefficients and imaginary parts of refractive indices of Saharan
11 dust during SAMUM-1. *Tellus*, 61B, 79-95, 2011.
- 12 Omar, A. H., Winker, D. M., Kittaka, C., Vaughan, M. A., Liu, Z. Y., Hu, Y. X.,
13 Trepte, C. R., Rogers, R. R., Ferrare, R. A., Lee, K. P., Kuehn, R. E., and
14 Hostetler, C. A.: The CALIPSO automated aerosol classification and lidar ratio selec-
15 tion algorithm, *J. Atmos. Ocean. Tech.*, 26, 1994–2014,
16 doi:10.1175/2009jtech1231.1, 2009.
- 17 O’Neill, N. T., Eck, T. F., Smirnov, A., Holben, B. N. and Thulasiraman, S.: Spectral
18 discrimination of coarse and fine mode optical depth, *J. Geophys. Res.*, 108(D17),
19 4559, 2003.
- 20 Omar, A. H., Winker, D. M., Tackett, J. L., Giles, D. M., Kar, J., Liu, Z., Vaughan,
21 M. A., Powell, K. A., and Trepte, C. R.: CALIOP and AERONET aerosol optical
22 depth comparisons: One size fits none, *J. Geophys. Res. Atmos.*, 118, 4748–4766,
23 doi:10.1002/jgrd.50330, 2013.
- 24 Omar, A. H., Won, J.-G., Winker, D. M., Yoon, S.-C., Dubovik, O. & Mc- Cormick,
25 M. P., Development of global aerosol models using cluster analysis of Aerosol Robot-
26 ic Network (AERONET) measurements, *J. Geophys. Res.*, 110, doi:
27 10.1029/2004JD004874. 177, 2005.
- 28 Pappalardo, G., A. Amodeo, M. Pandolfi, U. Wandinger, A. Ansmann, J. Bosenberg,
29 V. Matthias, V. Amiridis, F. De Tomasi, M. Frioud, M. Iarlori, L. Komguem, A. Pa-

1 payannis, F. Rocadenbosch, and X. Wang, Aerosol lidar intercomparison in the
2 framework of the EARLINET project. 3. Raman lidar algorithm for aerosol extinc-
3 tion, backscatter and lidar ratio, *Appl. Opt.*, 43. N. 28, 5370-5385, 2004.

4 Pappalardo, G., Wandinger, U., Mona, L., Hiebsch, A., Mattis, I., Amodeo, A.,
5 Ansmann, A., Seifert, P., Linne, H., Apituley, A., Alados Arboledas, L., Balis, D.,
6 Chaikovskiy, A., D'Amico, G., De Tomasi, F., Freudenthaler, V., Giannakaki, E.,
7 Giunta, A., Grigorov, I., Iarlori, M., Madonna, F., Mamouri, R.-E., Nasti, L., Papa-
8 yannis, A., Pietruczuk, A., Pujadas, M., Rizi, V., Rocadenbosch, F., Russo, F.,
9 Schnell, F., Spinelli, N., Wang, X., and Wiegner, M.: EARLINET correlative meas-
10 urements for CALIPSO: first intercomparison results, *J. Geophys. Res.*, 115,
11 D00H19, doi:10.1029/2009JD012147, 2010.

12 Pappalardo, G., Amodeo, A., Apituley, A., Comeron, A., Freudenthaler, V., Linné, H.,
13 Ansmann, A., Bösenberg, J., D'Amico, G., Mattis, I., Mona, L., Wandinger, U.,
14 Amiridis, V., Alados-Arboledas, L., Nicolae, D., and Wiegner, M.: EARLINET: to-
15 wards an advanced sustainable European aerosol lidar network, *Atmos. Meas. Tech.*
16 *Discuss.*, 7, 2929-2980, doi:10.5194/amtd-7-2929-2014, 2014.

17 Reid, J. S., Koppmann, R., Eck, T. F., and Eleuterio, D. P.: A review of biomass burn-
18 ing emissions part II: intensive physical properties of biomass burning particles, *At-*
19 *mos. Chem. Phys.*, 5, 799-825, doi:10.5194/acp-5-799-2005, 2005.

20 Sayer, A. M., A. Smirnov, N. C. Hsu, and B. N. Holben, A pure marine aerosol mod-
21 el, for use in remote sensing applications, *J. Geophys. Res.*, 117, D05213,
22 doi:10.1029/2011JD016689, 2012.

23 Schuster, G. L., Vaughan, M., MacDonnell, D., Su, W., Winker, D., Dubovik, O.,
24 Lapyonok, T., and Trepte, C.: Comparison of CALIPSO aerosol optical depth retriev-
25 als to AERONET measurements, and a climatology for the lidar ratio of dust, *Atmos.*
26 *Chem. Phys.*, 12 (16), 7431-7452, doi:10.5194/acp-12-7431-2012, 2012.

27 Smirnov, A., Holben, B. N., Kaufman, Y. J., Dubovik, O., Eck, T. F., Slutsker, I.,
28 Pietras, C., and Halthore, R. N.: Optical properties of atmospheric aerosol in maritime
29 environments. *J. Atmos. Sci.*, 59, 501–523, 2002.

1 Stoffelen, A., et al., The Atmospheric Dynamics Mission for Global Wind Field
2 Measurements, *Bull. Amer. Meteor. Soc.*, 86 (1), 73-87, 2005.

3 Tesche, M., Wandinger, U., Ansmann, A., Althausen, D., Müller, D., and Omar, A.H.:
4 Ground-based validation of CALIPSO observations of dust and smoke in the Cape
5 Verde region, *J. Geophys. Res.*, Vol. 118, 1–14, doi:10.1002/jgrd.50248, 2013.

6 The EARLINET publishing group 2000–2010: Adam, M., Alados-Arboledas, L., Al-
7 thausen, D., Amiridis, V., Amodeo, A., Ansmann, A., Apituley, A., Arshinov, Y.,
8 Balis, D., Belegante, L., Bobrovnikov, S., Boselli, A., Bravo-Aranda, J. A., Bösen-
9 berg, J., Carstea, E., Chaikovsky, A., Comerón, A., D’Amico, G., Daou, D.,
10 Dreischuh, T., Engelmann, R., Finger, F., Freudenthaler, V., Garcia-Vizcaino, D.,
11 García, A. J. F., Geiß, A., Giannakaki, E., Giehl, H., Giunta, A., de Graaf, M., Grana-
12 dos-Muñoz, M. J., Grein, M., Grigorov, I., Groß, S., Gruening, C., Guerrero-Rascado,
13 J. L., Haeffelin, M., Hayek, T., Iarlori, M., Kanitz, T., Kokkalis, P., Linné, H., Ma-
14 donna, F., Mamouriat, R.-E., Matthias, V., Mattis, I., Menéndez, F. M., Mitev, V.,
15 Mona, L., Morille, Y., Muñoz, C., Müller, A., Müller, D., Navas-Guzmán, F., Nemuc,
16 A., Nicolae, D., Pandolfi, M., Papayannis, A., Pappalardo, G., Pelon, J., Perrone, M.
17 R., Pietruczuk, A., Pisani, G., Potma, C., Preißler, J., Pujadas, M., Putaud, J., Radu,
18 C., Ravetta, F., Reigert, A., Rizi, V., Rocadenbosch, F., Rodríguez, A., Sauvage, L.,
19 Schmidt, J., Schnell, F., Schwarz, A., Seifert, P., Serikov, I., Sicard, M., Silva, A. M.,
20 Simeonov, V., Siomos, N., Sirch, T., Spinelli, N., Stoyanov, D., Talianu, C., Tesche,
21 M., De Tomasi, F., Trickl, T., Vaughan, G., Volten, H., Wagner, F., Wandinger, U.,
22 Wang, X., Wiegner, M., and Wilson, K. M.: EARLINET all observations (2000–
23 2010), World Data Center for Climate (WDCC),
24 doi:10.1594/WDCC/EN_all_measurements_2000-2010, 2014a.

25 The EARLINET publishing group 2000–2010: Adam, M., Alados-Arboledas, L., Al-
26 thausen, D., Amiridis, V., Amodeo, A., Ansmann, A., Apituley, A., Arshinov, Y.,
27 Balis, D., Belegante, L., Bobrovnikov, S., Boselli, A., Bravo-Aranda, J. A., Bösen-
28 berg, J., Carstea, E., Chaikovsky, A., Comerón, A., D’Amico, G., Daou, D.,
29 Dreischuh, T., Engelmann, R., Finger, F., Freudenthaler, V., Garcia-Vizcaino, D.,
30 García, A. J. F., Geiß, A., Giannakaki, E., Giehl, H., Giunta, A., de Graaf, M., Grana-
31 dos-Muñoz, M. J., Grein, M., Grigorov, I., Groß, S., Gruening, C., Guerrero-Rascado,
32 J. L., Haeffelin, M., Hayek, T., Iarlori, M., Kanitz, T., Kokkalis, P., Linné, H., Ma-

1 donna, F., Mamouriat, R.E., Matthias, V., Mattis, I., Menéndez, F. M., Mitev, V.,
2 Mona, L., Morille, Y., Muñoz, C., Müller, A., Müller, D., Navas-Guzmán, F., Nemuc,
3 A., Nicolae, D., Pandolfi, M., Papayannis, A., Pappalardo, G., Pelon, J., Perrone,
4 M.R., Pietruczuk, A., Pisani, G., Potma, C., Preißler, J., Pujadas, M., Putaud, J., Radu,
5 C., Ravetta, F., Reigert, A., Rizi, V., Rocadenbosch, F., Rodríguez, A., Sauvage, L.,
6 Schmidt, J., Schnell, F., Schwarz, A., Seifert, P., Serikov, I., Sicard, M., Silva, A. M.,
7 Simeonov, V., Siomos, N., Sirch, T., Spinelli, N., Stoyanov, D., Talianu, C., Tesche,
8 M., De Tomasi, F., Trickl, T., Vaughan, G., Volten, H., Wagner, F., Wandinger, U.,
9 Wang, X., Wiegner, M., and Wilson, K. M.: EARLINET climatology (2000–2010),
10 World Data Center for Climate (WDCC),
11 doi:10.1594/WDCC/EN_Climatology_2000-2010, 2014b.

12 The EARLINET publishing group 2000–2010: Adam, M., Alados-Arboledas, L., Al-
13 thausen, D., Amiridis, V., Amodeo, A., Ansmann, A., Apituley, A., Arshinov, Y.,
14 Balis, D., Belegante, L., Bobrovnikov, S., Boselli, A., Bravo-Aranda, J. A., Bösen-
15 berg, J., Carstea, E., Chaikovsky, A., Comerón, A., D’Amico, G., Daou, D.,
16 Dreischuh, T., Engelmann, R., Finger, F., Freudenthaler, V., Garcia-Vizcaino, D.,
17 García, A. J. F., Geiß, A., Giannakaki, E., Giehl, H., Giunta, A., de Graaf, M., Grana-
18 dos-Muñoz, M. J., Grein, M., Grigorov, I., Groß, S., Gruening, C., Guerrero-Rascado,
19 J. L., Haeffelin, M., Hayek, T., Iarlori, M., Kanitz, T., Kokkalis, P., Linné, H., Ma-
20 donna, F., Mamouriat, R.-E., Matthias, V., Mattis, I., Menéndez, F. M., Mitev, V.,
21 Mona, L., Morille, Y., Muñoz, C., Müller, A., Müller, D., Navas-Guzmán, F., Nemuc,
22 A., Nicolae, D., Pandolfi, M., Papayannis, A., Pappalardo, G., Pelon, J., Perrone, M.
23 R., Pietruczuk, A., Pisani, G., Potma, C., Preißler, J., Pujadas, M., Putaud, J., Radu,
24 C., Ravetta, F., Reigert, A., Rizi, V., Rocadenbosch, F., Rodríguez, A., Sauvage, L.,
25 Schmidt, J., Schnell, F., Schwarz, A., Seifert, P., Serikov, I., Sicard, M., Silva, A. M.,
26 Simeonov, V., Siomos, N., Sirch, T., Spinelli, N., Stoyanov, D., Talianu, C., Tesche,
27 M., De Tomasi, F., Trickl, T., Vaughan, G., Volten, H., Wagner, F., Wandinger, U.,
28 Wang, X., Wiegner, M., and Wilson, K. M.: EARLINET correlative observations for
29 CALIPSO (2006–2010), World Data Center for Climate (WDCC),
30 doi:10.1594/WDCC/EN_Calipso_2006-2010, 2014c.

31 The EARLINET publishing group 2000-2010, Adam, M., Alados-Arboledas, L., Al-
32 thausen, D., Amiridis, V., Amodeo, A., Ansmann, A., Apituley, A., Arshinov, Y.,

1 Balis, D., Belegante, L., Bobrovnikov, S., Boselli, A., Bravo-Aranda, J. A., Bösen-
2 berg, J., Carstea, E., Chaikovsky, A., Comerón, A., D'Amico, G., Daou, D.,
3 Dreischuh, T., Engelmann, R., Finger, F., Freudenthaler, V., Garcia-Vizcaino, D.,
4 García, A. J. F., Geiß, A., Giannakaki, E., Giehl, H., Giunta, A., de Graaf, M., Grana-
5 dos-Muñoz, M. J., Grein, M., Grigorov, I., Groß, S., Gruening, C., Guerrero-Rascado,
6 J. L., Haeffelin, M., Hayek, T., Iarlori, M., Kanitz, T., Kokkalis, P., Linné, H., Ma-
7 donna, F., Mamouriat, R.-E., Matthias, V., Mattis, I., Menéndez, F. M., Mitev, V.,
8 Mona, L., Morille, Y., Muñoz, C., Müller, A., Müller, D., Navas-Guzmán, F., Nemuc,
9 A., Nicolae, D., Pandolfi, M., Papayannis, A., Pappalardo, G., Pelon, J., Perrone, M.
10 R., Pietruczuk, A., Pisani, G., Potma, C., Preißler, J., Pujadas, M., Putaud, J., Radu,
11 C., Ravetta, F., Reigert, A., Rizi, V., Rocadenbosch, F., Rodríguez, A., Sauvage, L.,
12 Schmidt, J., Schnell, F., Schwarz, A., Seifert, P., Serikov, I., Sicard, M., Silva, A. M.,
13 Simeonov, V., Siomos, N., Sirch, T., Spinelli, N., Stoyanov, D., Talianu, C., Tesche,
14 M., De Tomasi, F., Trickl, T., Vaughan, G., Volten, H., Wagner, F., Wandinger, U.,
15 Wang, X., Wiegner, M., and Wilson, K. M.: EARLINET observations related to vol-
16 canic eruptions (2000–2010), World Data Center for Climate (WDCC),
17 doi:10.1594/WDCC/EN_VolcanicEruption_2000-2010, 2014d.

18 The EARLINET publishing group 2000–2010: Adam, M., Alados-Arboledas, L., Al-
19 thausen, D., Amiridis, V., Amodeo, A., Ansmann, A., Apituley, A., Arshinov, Y.,
20 Balis, D., Belegante, L., Bobrovnikov, S., Boselli, A., Bravo-Aranda, J. A., Bösen-
21 berg, J., Carstea, E., Chaikovsky, A., Comerón, A., D'Amico, G., Daou, D.,
22 Dreischuh, T., Engelmann, R., Finger, F., Freudenthaler, V., Garcia-Vizcaino, D.,
23 García, A. J. F., Geiß, A., Giannakaki, E., Giehl, H., Giunta, A., de Graaf, M., Grana-
24 dos-Muñoz, M. J., Grein, M., Grigorov, I., Groß, S., Gruening, C., Guerrero-Rascado,
25 J. L., Haeffelin, M., Hayek, T., Iarlori, M., Kanitz, T., Kokkalis, P., Linné, H., Ma-
26 donna, F., Mamouriat, R.-E., Matthias, V., Mattis, I., Menéndez, F. M., Mitev, V.,
27 Mona, L., Morille, Y., Muñoz, C., Müller, A., Müller, D., Navas-Guzmán, F., Nemuc,
28 A., Nicolae, D., Pandolfi, M., Papayannis, A., Pappalardo, G., Pelon, J., Perrone, M.
29 R., Pietruczuk, A., Pisani, G., Potma, C., Preißler, J., Pujadas, M., Putaud, J., Radu,
30 C., Ravetta, F., Reigert, A., Rizi, V., Rocadenbosch, F., Rodríguez, A., Sauvage, L.,
31 Schmidt, J., Schnell, F., Schwarz, A., Seifert, P., Serikov, I., Sicard, M., Silva, A. M.,
32 Simeonov, V., Siomos, N., Sirch, T., Spinelli, N., Stoyanov, D., Talianu, C., Tesche,
33 M., De Tomasi, F., Trickl, T., Vaughan, G., Volten, H., Wagner, F., Wandinger, U.,

- 1 Wang, X., Wiegner, M., and Wilson, K. M.: EARLINET observations related to Sa-
2 haran Dust events (2000–2010), World Data Center for Climate (WDCC),
3 doi:10.1594/WDCC/EARLINET_SaharanDust_2000-2010, 2014e. Toledano, C.,
4 Wiegner, M., Gross, S., Freudenthaler, V., Gasteiger, J., Müller, D., Müller, T.,
5 Schladitz, A., Weinzierl, B., Torres B., and O'Neill, N. T.: Optical properties of aero-
6 sol mixtures derived from sun-sky radiometry during SAMUM-2. *Tellus* 63B, 635-
7 648, doi: 10.1111/j.1600-0889.2011.00573.x, 2011.
- 8 Van de Hulst, H., *Light Scattering by Small Particles*, New York: Wiley, 1957.
- 9 Vaughan, J.M., Geddes, N.J., Flamant P.H., and Flesia C., Establishment of a
10 backscatter coefficient and atmospheric database, DERA Report for ESA Contract no.
11 12510/97/NL/RE, DERA/EL/ISET/CR980139/1.0, 1998.
- 12 Vaughan, M. A., Powell, K. A., Kuehn, R. E., Young, S. A., Winker, D. M.,
13 Hostetler, C. A., Hunt, W. H., Liu, Z. Y., McGill, M. J., and Getzewich, B. J.: Fully
14 automated detection of cloud and aerosol layers in the CALIPSO lidar measurements,
15 *J. Atmos. Ocean. Tech.*, 26, 2034–2050, doi:10.1175/2009jtecha1228.1, 2009.
- 16 Volten, H., O. Munoz, E. Rol, J. F. de Haan, W. Vassen, J. W. Hovenier, K. Mui-
17 nonen, and T. Nousiainen: Scattering matrices of mineral aerosol particles at 441.6
18 nm and 632.8 nm, *J. Geophys. Res.*, 106, 17, 375–17, 401, 2001.
- 19 Wandinger, U., Ansmann, A., Reichardt, J., Deshler, T., Determination of stratospher-
20 ic aerosol microphysical properties from independent extinction and backscattering
21 measurements with a Raman lidar, *Appl Opt.*, 34(36), 8315-29. doi:
22 10.1364/AO.34.008315, 1995.
- 23 Wandinger, U., Tesche, M., Seifert, P., Ansmann, A., Müller, D., and Althausen, D.:
24 Size matters: Influence of multiple scattering on CALIPSO light-extinction profiling
25 in desert dust, *Geophysical Research Letters*, 37 (10), L10801, doi:
26 10.1029/2010GL042815, 2010.
- 27 Wandinger U., Hiebsch, A., Mattis, I., Pappalardo, G., Mona, L., and Madonna F.,
28 *Aerosols and Clouds: Long-term Database from Spaceborne Lidar Measurements*,

1 Executive Summary, <http://esamultimedia.esa.int/docs/gsp/C21487ExS.pdf>, ESTEC
2 Contract 21487/08/NL/HE, 2011.

3 Weinzierl, B., Petzold, A., Esselborn, M., Wirth, M., Rasp, K., Kandler, K., Schütz,
4 L., Koepke P., and Fiebig, M.: Airborne measurements of dust layer properties, parti-
5 cle size distribution and mixing state of Saharan dust during SAMUM 2006. *Tellus*
6 61B, 96-117 doi: 10.1111/j.1600-0889.2008.00392.x, 2009.

7 Winker, D. M., Vaughan, M. A., Omar, A., Hu, Y., Powell, K. A., Liu, Z., Hunt, W.
8 H., and Young, S. A.: Overview of the CALIPSO mission and CALIOP data pro-
9 cessing algorithms, *J. Atmos. Ocean. Tech.*, 26, 2310–2323, doi:
10 10.1175/2009JTECHA1281.1, 2009.

11 Winker, D. M., Tackett, J. L., Getzewich, B. J., Liu, Z., Vaughan, M. A., and Rog-
12 ers, R. R.: The global 3-D distribution of tropospheric aerosols as characterized by
13 CALIOP, *Atmos. Chem. Phys.*, 13, 3345-3361, doi:10.5194/acp-13-3345-2013,
14 2013.

15 Yang, P., and K. N. Liou, Geometric-optics-integral-equation method for light scatter-
16 ing by nonspherical ice crystals, *Appl. Opt.*, 35, 6568–6584, 1996.

17 Young, S.A., and Vaughan, M. A.: The retrieval of profiles of particulate extinction
18 from cloud-aerosol lidar infrared pathfinder satellite observations (CALIPSO) data:
19 Algorithm description, *J. Atmos. Oceanic Techn.*, 26 (6), pp. 1105-1119, doi:
20 10.1175/2008JTECHA1221.1, 2009.

21
22